Nano Today 26 (2019) 123–148

Contents lists available at ScienceDirect

Nano Today

journal homepage: www.elsevier.com/locate/nanotoday

Review

Nanofabrication based on DNA nanotechnology

Yan Zhao[a], Xinpei Dai[a], Fei Wang[b,c], Xueli Zhang[b], Chunhai Fan[a,c,*], Xiaoguo Liu[c,*]

[a] Division of Physical Biology & Bioimaging Center, Shanghai Synchrotron Radiation Facility, Shanghai Institute of Applied Physics, Chinese Academy of Sciences, University of Chinese Academy of Sciences, Shanghai 201800, PR China
[b] Joint Research Center for Precision Medicine, Shanghai Jiao Tong University & Affiliated Sixth People's Hospital South Campus, Fengxian Hospital, Shanghai 201499, PR China
[c] School of Chemistry and Chemical Engineering, Institute of Molecular Medicine, Renji Hospital, School of Medicine, Shanghai Jiao Tong University, Shanghai 200240, PR China

ARTICLE INFO

Article history:
Received 29 December 2018
Received in revised form 31 January 2019
Accepted 18 March 2019
Available online 28 March 2019

Keywords:
Nanofabrication
DNA nanostructures
Plasmonic devices
Drug delivery
Biodetection

ABSTRACT

Nanofabrication refers to manufacturing objects with nanometer dimensions. The evolution of DNA nanotechnology has brought new inspirations to this field, owing to the unprecedented programmability of DNA molecules. By combining with other components, DNA nanostructures can template the growth of heterogeneous materials, support delicate plasmonic devices, build smart drug delivery vehicles and detect biomolecular targets. This article focuses on key strategies for DNA-based nanofabrication and highlights recent developments in chemical reactions confined on DNA nanostructures, including metallization, mineralization and polymer coating. We also review applications based on DNA nanofabrication and propose perspective in this field.

Contents

* Corresponding author at: School of Chemistry and Chemical Engineering, Institute of Molecular Medicine, Renji Hospital, School of Medicine, Shanghai Jiao Tong University, Shanghai 200240, PR China.
E-mail addresses: fanchunhai@sjtu.edu.cn (C. Fan), liuxiaoguo@sjtu.edu.cn (X. Liu).

https://doi.org/10.1016/j.nantod.2019.03.004
1748-0132/

Introduction

Manufacturing accuracy is a critical indicator to the civilization degree. The fabrication of all devices is generally divided into two approaches, 'top-down' versus 'bottom-up' [1,2]. The top-down method is widely adopted in industrial manufacturing, it begins with entire structures and machines to desired scales and patterns through external tools, for example, lathe processing for metal parts and lithography techniques in semiconductors. Currently, it is possible to create transistors with process precision down to 7 nm [3] through extreme ultraviolet lithography. But lithography is strictly restricted to certain substrates such as silicon oxide (also terms as silica), also the difficulties increase in geometric multiples for smaller structures at molecular or even atomic scale, and these are common problems in all top down methods. In contrast, the bottom-up method follows nature's rules, it uses intermolecular interactions, including but not limited to hydrogen bond, π-π stacking, Van Der Waals and electrostatic forces, to guide the self-assembly of molecules and units. Various delicate organisms such as bone, enamel, shells and butterfly wings are constructed through this way, which far exceed any existed top-down manufactured devices in their structural complexity and functions. However, even though intense studies have been carried out in this field [4–6], the artificial assembly of molecules into user-defined arrangements expanding from nanoscale to macroscale, which is critical for their final function, is particularly challenging.

The blooming DNA nanotechnology has revolutionarily changed the bottom-up nanofabrication [7–9]. The robust Watson-Crick base pairing rule (A–T, C–G) makes it possible for DNA to specifically bind to each other and fold into almost infinite structures, which surpasses any existed natural or synthetic molecule [10]. The simple functional groups of nucleic acids allow them to predictably interact with diverse heterogeneous components, either by negatively charged phosphate backbones or nucleobases that can chelate metal ions and form π-stacking [11]. These also guaranteed the rapid synthesizing and modification of DNA. DNA double helix is structurally well defined and has a persistence length of ~50 nm, which ensures the fabrication accuracy within only a few nanometers. The theoretical structural accuracy provided by DNA along the helices could reach 0.34 nm, which is determined by the distance between two adjacent bases. While the accuracy on the direction perpendicular to the helices is about 2 nm, which is restricted by the diameter of DNA double helix. In addition, DNA has good thermal stability [12] and can withstand a temperature up to 95 °C, as well as a wide pH tolerance range between 4 and 11. RNA also functions as an information carrier in cells, which plays important roles in the regulation of gene expressions and other functions. In recent years, researchers have taken interests in designing and constructing RNA nanostructures [13]. As RNA is chemically similar to DNA, through minor modulations, the orthodox Watson-Crick base-pairing strategies could be applied to design RNA nanostructures. Up to now, various RNA structures have been developed, such as a cubic wireframe structure [14], ribbon-, rectangle- or triangle-shaped RNA origami structures [15]. In addition, RNA can form RNA structural motifs through other inter- and intra-molecular interactions including non-canonical base-pairing, base-ribose and base-phosphate interaction [16]. With these motifs, RNA nanostructures with a relatively small size scale can be developed [17,18]. These nanostructures have been served as powerful tools in biological research, bioengineering and further medicine [19]. However, RNA will be easily degraded by nuclease, which limits its developments and applications (Scheme 1).

In this article, we aim to give a staged review over the developments of nanofabrication based on DNA nanotechnology in the past decades. We will first look back to the history of building DNA nanostructures from simple units to complex assemblies, which provides the necessary frameworks for nanofabrication. Then we will discuss the basic ideas of using DNA structures in nanofabrication, including assembling materials with DNA and direct chemical reaction on DNA. After that, we will summarize the most inspiring biophysical, biomedical, physical and material applications relied on DNA nanofabrication. Despite the above advantages and many encouraging demonstrations, we will finally have an inspection over this filed, discuss the challenges and draw insights from these pioneered explorations.

DNA nanostructures scale-up

Scaling up of DNA nanostructures is of vital importance for DNA-based nanofabrication, it offers basic frameworks for subsequent handling and bridges from the bottom to the top. The "bottom-up" fabricated DNA nanostructures exploits the hybridization of single-stranded DNA (ssDNA) to self-assemble into arbitrary shapes. High-order and large-scale nanostructures could be precisely assembled via three major routes: sticky-end cohesion, base-pair stacking and scaffold extension. Early works utilized DNA tiles, which include the single stranded tile (SST) [43], n-arm junction [44–47], double crossover tile (DX) [22,48] and cross tile [49]. In 2006, Rothemund proposed a milestone technique named DNA origami [23], of which, a 7-kilobase single-stranded scaffold was folded into various two dimensional (2D) nanostructures with the help of hundreds of staple strands. Later, the concept of "DNA bricks" was presented by Yin et al. in 2012 [20]. Similar to the SST, "DNA bricks" are single strands composed of several binding domains. Compared to SST, "DNA bricks" are 3D structural motifs. The extended ssDNA scaffold would also be helpful in assembling larger DNA nanostructures. Yan et al. utilized double stranded DNA (dsDNA) scaffolds to fabricate DNA origami, in which the dsDNA scaffold served as two ssDNA strands aligned head to tail [25]. Labean et al. produced 51 kilobases ssDNA scaffolds derived from λ/M13 hybrid phages. After adding 1600 staples, the edge length of the folded rectangle was 400 nm [27]. Possessing a spatial resolution of 5 nm, DNA nanostructures with large-scale dimension lay the foundation to nanofabrication.

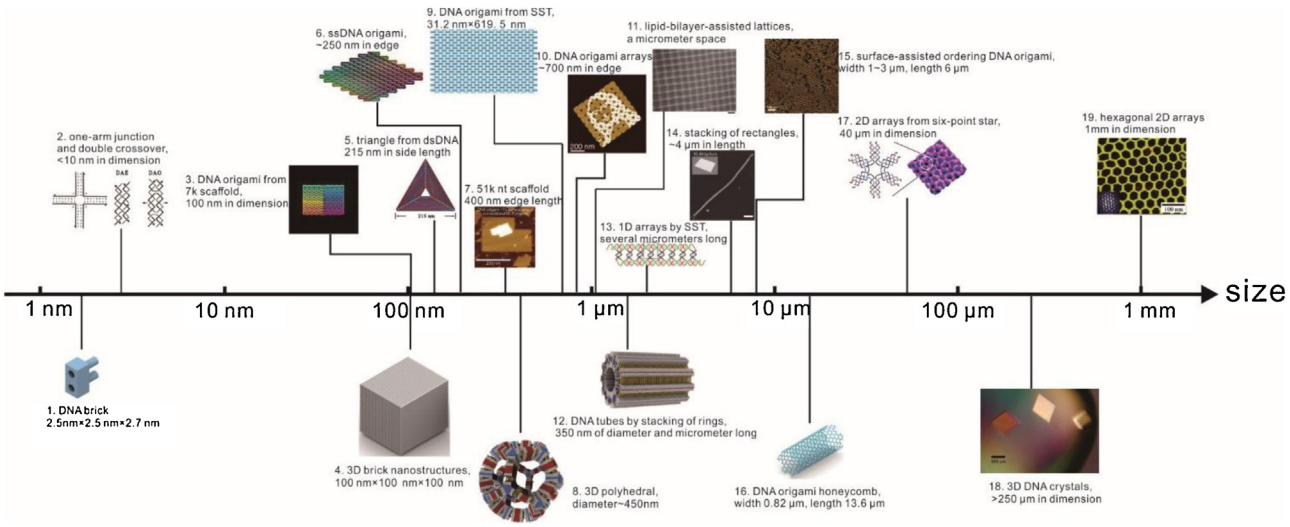

Scheme 1. A scale ruler of various DNA structures. Structural motif (≤ 100 nm): (1) DNA bricks with dimension of 2.5 nm × 2.5 nm × 2.7 nm. Reprinted with permission from ref. [20] Copyright © 2012, The American Association for the Advancement of Science. (2) 2D DNA tiles including one-arm junction and double crossover. Reprinted with permission from ref. [21,22] Copyright © 1997 and 1993, American Chemical Society. (3) DNA origami folded by a ~7k scaffold and 200 staple strands, with arbitrary shapes nearly 100 nm. Reprinted with permission from ref [23]. Copyright © 2006, Springer Nature. Large-scale DNA nanostructures (100 nm~1 mm): (4) 3D nanostructures assembled by ~30,000 DNA bricks, dimensions of 100 nm × 100 nm × 100 nm. Reprinted with permission from ref [24]. Copyright © 2017, Springer Nature. (5) Large triangle origami folded by dsDNA scaffold. Reprinted with permission from ref [25]. Copyright © 2012, American Chemical Society. (6) 10,682 nt single stranded DNA origami. Reprinted with permission from ref [26]. Copyright © 2017, American Association for the Advancement of Science. (7) Rectangle origami made by 51k nt scaffold. Reprinted with permission from ref. [27] Copyright © 2014, American Chemical Society. (8) Polyhedral nanostructures with diameter of 450 nm. Reprinted with permission from ref [28]. Copyright © 2017, Springer Nature. (9) DNA origami conjugated by single-stranded tiles (SST). Reprinted with permission from ref [29]. Copyright © 2012, Springer Nature. (10) 2D DNA arrays with arbitrary patterns. Reprinted with permission from ref [30]. Copyright © 2017, Springer Nature. (11) Lipid-bilayer-assisted 2D DNA arrays. Reprinted with permission from ref [31]. Copyright © 2015, Springer Nature. (12) 3D DNA tubes stacking of ring oligomers. Reprinted with permission from ref [28]. Copyright © 2017, Springer Nature. (13) 1D DNA arrays assembled by SST. Reprinted with permission from ref [32]. Copyright © 2013, American Chemical Society. (14) Blunt-end stacking of DNA rectangles. Reprinted with permission from ref [33]. Copyright © 2011, Springer Nature. (15) Surface-assisted ordering DNA origami by electrochemical control. Reprinted with permission from ref. [34] Copyright © 2014, John Wiley and Sons. (16) DNA origami honeycomb tubes. Reprinted with permission from ref [35]. Copyright © 2016, American Chemical Society. (17) 2D DNA arrays conjugating from six-point-star motifs. Reprinted with permission from ref [36]. Copyright © 2006, American Chemical Society. (18) 3D DNA crystals assembling from tensegrity triangles. Reprinted with permission from ref [37]. Copyright © 2009, Springer Nature. (19) Hexagonal 2D DNA arrays assembling from three-point-star motifs. Reprinted with permission from ref [38]. Copyright © 2005, American Chemical Society.

Hybridization and sticky-end cohesion

The main idea of sticky-end cohesion is to hybridize extended complementary ssDNA on different motifs. The motifs can be single stranded tile (SST), n-arm junction, double crossover tile, DNA brick and DNA origami. DNA structures formed in this way could reach millimeter scale.

Yin and Mao group both constructed complex shapes with SST motif. In 2012, a 42-base SST was developed by Yin et al. [29]. Each SST was divided into four domains and folded into a 3 nm × 7 nm tile by attaching to other four neighboring tiles. Using one-pot annealing, the assembled 24 helices × 28 helical turns (24H × 28 T) rectangle from 362 SST could reach 64 nm × 103 nm, and (12H × 177 T) tube made from more than 1000 SST could reach 31.2 nm × 619.5 nm (Fig. 1a). The SST proposed by Mao et al. contained five domains: one central palindrome and two sets of complementary segments [32]. Two strands hybridize with each other to form a symmetric motif. Z- and C- shaped tiles were formed according to the even and odd number of half turns in central segments. After annealing from 95 °C to 22 °C, Z-shaped tiles assembled to 1D chains with lengths of several micrometers by surface-mediated assembly. C-shaped tiles could form 2D arrays and 1D nanotubes due to the flexibility of 2D arrays. Yin et al. synthesized multi-kilobase ssDNA by polymerase Chain Reaction (PCR) [26]. These single DNA strands could be folded into various unknotted ssDNA origami (Fig. 1b). In their work, the ~10,000 bases DNA structure was 37 times larger than previous reports.

Three-, four-, six-arm junctions could conjugate by sticky ends to self-assemble into 1D and 2D DNA arrays. Mao et al. developed three-point-star [38] and six-point-star [36] DNA motifs to fabricate 2D DNA arrays. The 2D arrays assembled by three-point-star motifs were as large as 1 mm. Six-point-star motif with 12 sticky-ends made the subsequent arrays more tough (Fig. 1c), and the arrays reached 40 μm. They also constructed rigid DNA triangles by four-arm junctions, where each triangle was fused by three four-arm junctions [50]. Adding a pair of sticky ends to one side of the triangle would form 1D arrays, while two pairs of sticky ends resulted in 2D periodic arrays.

Planar DNA origami with protruding sticky ends could hybridize into larger 2D structures. Qian et al. designed a square origami tile composed of four triangles [39]. Each edge consists of four staples, and each staple has a stacking bond and a two-base sticky-end. The assembled 10 × 10 arrays reached 880 × 880 nm^2. Three patterns (random loops, mazes and trees) displayed on the surface of DNA arrays with nanometer resolution. Subsequently, in order to display more sophisticated patterns on 8 × 8 arrays, they developed the "fractal assembly" method, which utilized a three-stage self-assembly process [30]. The maximum resolution of this array reached 8704 pixels, as demonstrated by the Mona Lisa (Fig. 1d) and rooster images. Recently, they showed triangle tiles could be assembled into 2D arrays up to 3.5 by 4.5 μm [51]. Ke et al. reported DNA-origami hexagon tiles with six protruding arms could self-assemble into 2D planar lattices or nanotubes spanning hundreds of nanometers to micrometers [35].

3D DNA motifs can also form a densely ordered arrangements through sticky-end hybridization. Yin et al. constructed complex 3D nanostructures with "DNA bricks" in a prescribed way [20]. Each brick contains four 8-base binding domains and has a dimension of 2.5 × 2.5 × 2.7 nm^3. Two neighboring bricks could bind to each other in a vertical orientation, thus 3D structures with 10 × 10 × 10 motifs could be fabricated, namely molecular canvas. By selecting subsets from this canvas, 102 distinct shapes were constructed

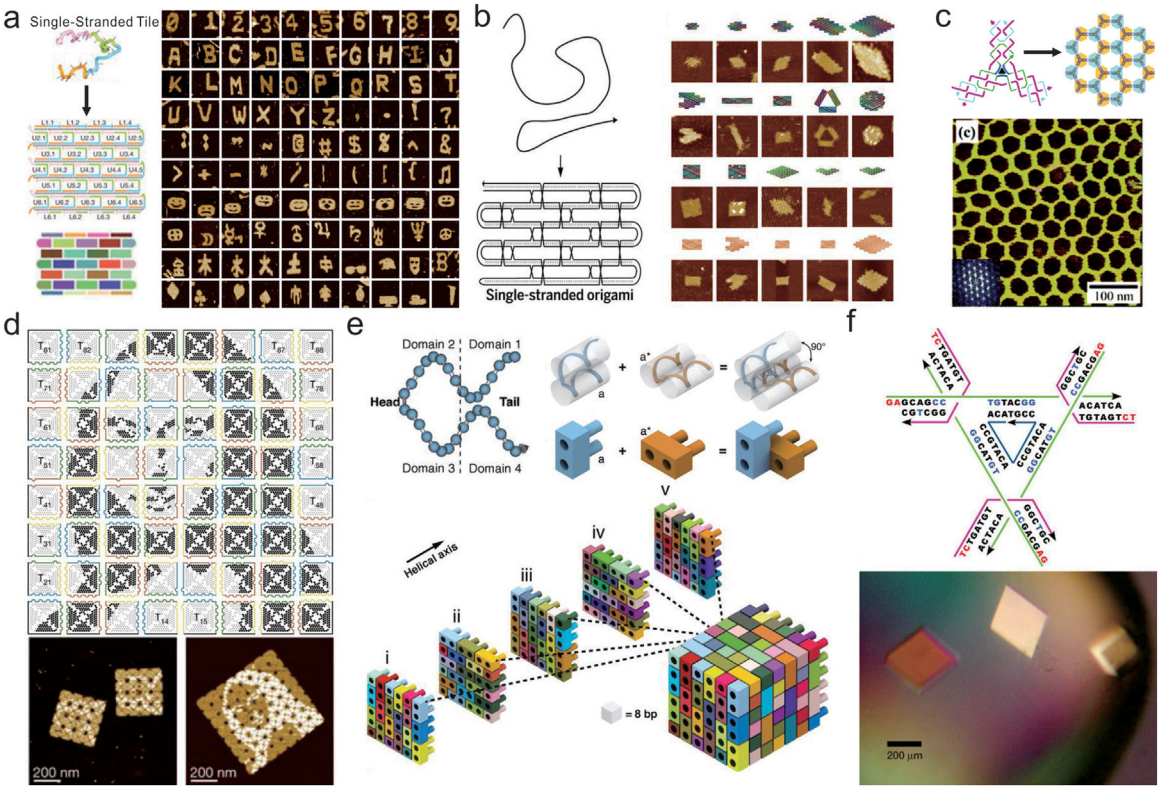

Fig. 1. Scale-up DNA nanostructures by sticky-end cohesion. a) Self-assembly of complex structures by single-stranded tiles. Reprinted with permission from ref. [29] Copyright © 2012, Springer Nature. b) Single-stranded DNA origami with prescribed shapes. Reprinted with permission from ref [26]. Copyright © 2017, American Association for the Advancement of Science. c) Self-assembly of hexagonal DNA 2D arrays. Reprinted with permission from ref [38]. Copyright © 2005, American Chemical Society. d) Fractal assembly of DNA origami arrays with arbitrary patterns. Reprinted with permission from ref [30]. Copyright © 2017, Springer Nature. e) 3D DNA nanostructures self-assembled from DNA bricks. Reprinted with permission from ref [20]. Copyright © 2012, American Association for the Advancement of Science. f) 3D DNA crystals based on tensegrity triangles. Reprinted with permission from ref [37]. Copyright © 2009, Springer Nature.

(Fig. 1e). Moreover, they developed larger structures with 52-base bricks containing four 13-base binding domains [24]. And the 3D nanostructures with molecule weights of 0.1∼1-gigadalton were assembled from tens of thousands of bricks.

The foundational goal of DNA nanotechnology is using nucleic acids as building blocks to construct 3D lattices for solving protein structures. Self-assembled 2D and 3D crystalline structures can immobilize guest molecules in a highly ordered array. Motifs associated with sticky ends without sharing the same plane could self-assemble into 3D DNA crystal. In 2009, Seeman et al. developed 3D DNA crystals with a resolution of ∼4 Å [37]. The structural motif is a tensegrity triangle consists three helices. One motif could connect with other six motifs to yield a 3D periodic lattice exceeding 250 μm (Fig. 1f). Subsequently, they maximized the resolution of crystals by modifying phosphate groups at 5'-end of the strands, and improved the stability of crystals to resist the low ionic strength by adding triplex-forming strands at the inter-units [52]. Yan et al. assembled 2D and 3D DNA crystals through the combination of layered-crossover tiles [40]. By hybridizing sticky ends at terminals, these tiles could assemble into 2D periodic lattice with controlled angles varying from 20° to 80°. Moreover, with some structural modifications, 3D crystals up to several hundred micrometers were assembled. They also created 3D DNA crystals with hexagonal lattice [41].

Base-pair stacking

Base-pair stacking between the adjacent duplex is the dominant stabilizing factor in DNA binding, and it is highly sequence-dependent: a GC/CG pair is stronger than the AT/TA pair. The reason why two complementary strands can bind may be that: base-pair stacking provides the binding enthalpy for duplex, and base pairing enforces specificity. In 2011, Rothemund et al. proposed the geometric arrangement of blunt-end stacking of DNA origami with two approaches: binary codes and shape complementarity [33]. The assembled 32-helix rectangle enabled 16-bit binary codes: an active patch (1') composed of G/C pairs used for base-pair stacking and inactive patch (0') with a ssDNA loop could adjust the accuracy of combination (Fig. 2a).

Increasing ion concentrations improves the assemblies of nanostructures with blunt ends. Simmel et al. arranged large-scale and ordered DNA origami by electrostatically controlled adhesion and mobility of DNA origami on mica surfaces [34]. Mg^{2+} ions serve as salt bridge between mica and origami, but monovalent ions (such as Na^{+}) would weaken this interaction. Thus, the origami structures with blunt-end could move on the surface and form close-packed structures. For example, the lattice domain assembled from cross-shaped origami had a length about 6 μm and a width of 1∼3 μm (Fig. 2b). Similar to this method, rectangular origami with blunt-end helices at the four corners were assembled into 2D checkboard lattices on mica surface [53]. Attributing to the cationic radius or enthalpies of hydration or specific complexation of ions with DNA or mica, Ni^{2+} exhibited stronger binding of DNA to mica than Mg^{2+}. Thus, the strong-to-weak binding transitions were that: at first, origami was immobilized on mica at 12.5 mM Mg^{2+}; then was diffused and formed lattices with adding 700 mM Na^{+}; subsequently, 1 mM Ni^{2+} was used to stop diffusion and immobilize the resulting lattices; last, the residual Na + was

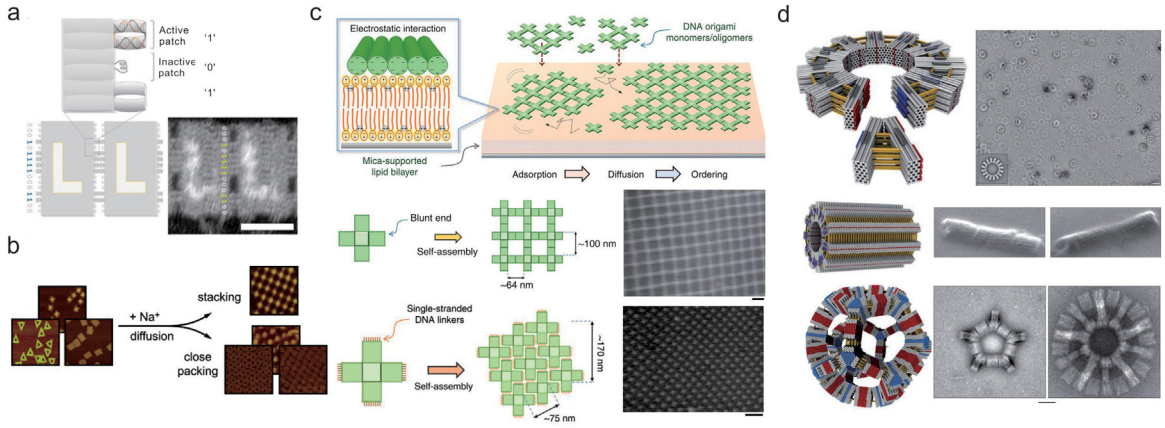

Fig. 2. Large-scale DNA arrays forming by base-pair stacking. a) Molecule recognition of DNA nanostructures based on geometric arrangements of stacked blunt ends. Reprinted with permission from ref. [33] Copyright © 2011, Springer Nature. b) Electrostatically ordering of large-scale DNA origami on surface. Reprinted with permission from ref [34]. Copyright © 2014, John Wiley and Sons. c) Lipid-bilayer-assisted 2D DNA lattices. Reprinted with permission from ref [31]. Copyright © 2015, Springer Nature. d) Shape-programmable self-assembling of ring oligomerization by multiple DNA V bricks. Reprinted with permission from ref [28]. Copyright © 2017, Springer Nature.

removed by 12.5 mM Mg^{2+}.Through stepwise control on ionic conditions (Mg^{2+}-Na^{+}-Ni^{2+}-Mg^{2+}), more than 90% rectangles were incorporated into lattices. Sugiyama et al. provided a strategy of "lipid bilayer-assisted self-assembly" to assemble DNA origami into micrometer-sized 2D lattices [31]. The DNA origami were electrostatically adsorbed on zwitterionic lipid bilayers in the presence of divalent cations, such as Mg^{2+} and Ca^{2+}, then they moved and self-assembled into large lattices on the lipid surface. Notably, the cross-shaped DNA origami with T4 (four thymine bases) ssDNA strands on the four edges could form close-packed structures (Fig. 2c). Recently, Dietz et al. produced gigadalton (GDa)-scale 3D DNA nanostructures with programmable shapes [28]. First, wedge-shaped building blocks ('V bricks') were fabricated through two interlocking self-complementary opposite surfaces. Then planar ring would assemble from the V bricks through increasing ionic strength. Eventually, after protruding docking sites perpendicular to the ring on V bricks and increasing ionic strength again, the ring could stack on each other to form long tubes with diameter of 350 nm and length over 1 μm. Moreover, hierarchical assembly of closed polyhedra was realized with a molecule weight of 1.2 GDa and a radius of 220 nm (Fig. 2d).

3D DNA crystals could also be formed by blunt-end stacking. High structural rigidity and large open space are important for DNA origami building blocks to arrange guest materials. Inspired by Seeman's 3D crystal design, Liedl et al. developed a DNA-origami-based "tensegrity triangle" motif to assemble 3D rhombohedral crystals [42]. Each triangle motif was constructed by three 14-helix bundles through triple over-under fashion. Then the motifs were conjugated by blunt-end stacking into micrometer scale 3D rhombohedral polycrystalline. A single domain was up to 2.5 μm^2 with a cavity size of 1.83×10^5 nm^3.

Principles of DNA nanofabrication

Assembling heterogeneous materials with DNA

Diverse fabrication techniques produced nanomaterials with variable shapes, sizes and compositions from inorganic or organic materials. DNA nanostructures have been used as templates for assembling these materials into unprecedent complex superstructures through programable hybridization. The key challenges are surface modification of these materials with DNA. In this section, we concluded the strategies of covalently attaching DNA onto the surface of inorganic materials and biological molecules.

Inorganic nanomaterials

Typical inorganic nanomaterials include metal and semiconductor nanoparticles, nanowires, nanosheets and nanorods. Decorating these materials with DNA mainly through covalent interactions and special affinity between nucleic acids and targeted nanomaterials [54].

Gold nanomaterials, such as gold nanoparticle (AuNP), gold nanotriangle and gold nanorod (AuNR) were synthesized under aqueous conditions with a coordinated shell of adsorbate (for example, citrate) [55]. They can be densely functionalized with thiols-modified DNA strands, which have a high affinity for gold. Liu et al. proposed various methods for attaching thiols-DNA (SH-DNA) to AuNPs [56]. There are mainly three strategies to promote the covalent modification of SH-DNA and AuNP (Fig. 3a): 1) salt-aging, AuNP was initially mixed with SH-DNA in water, and the gradually increased ionic strength could reduce the charge repulsion between negatively charged AuNP and oligonucleotides, which allowed more SH-ssDNA to attach onto the nanoparticle surface [57,58]. 2) pH-assisted, a low pH buffer rendered quantities DNA adsorption on AuNP surface by just a few minutes, compared to 1–2 days of salt aging protocol. At pH 3, A and C bases are positively charged, thus reducing the repulsion between AuNP and DNA, and allowing for fast adsorption [59]. 3) freezing-directed, DNA could be conjugated to AuNP during under -20 °C for two minutes, without addition of any other reagents. The DNA loading rate was 20–30% higher than salt-aging method. As temperature decreased, the crystallization of water molecules pushed AuNP, DNA and salt out of the crystals, which resulted in a high local concentration and enhancing the reaction rate [60].

For other nanomaterials synthesized in organic reagents, Mirkin et al. developed a general two-step approach to create a high-density ssDNA shell on nanoparticles with various compositions [61]. 1) Hydrophobic-ligand-protected nanoparticles were coated with azide-bearing amphiphilic polymer, which contained both hydrophobic alkyl chains to intercalate the hydrophobic ligands on nanoparticles, and hydrophilic carboxylates & azide modified groups to solubilize particles in aqueous conditions. 2) Dibenzocyclooctyl-terminated nucleic acids interacted with nanoparticles to produce a densely packed DNA shell around the nanoparticles through azide-alkyne click chemistry. In their work, multiple inorganic nanoparticle cores were demonstrated, including oleylamine-protected CdSe/ZnS quantum dots (QDs), dodecanethiol-functionalized AuNP, oleic acid-protected iron oxide nanoparticles (Fe_3O_4) and oleylamine-protected platinum nanoparticles (Pt) (Fig. 3b).

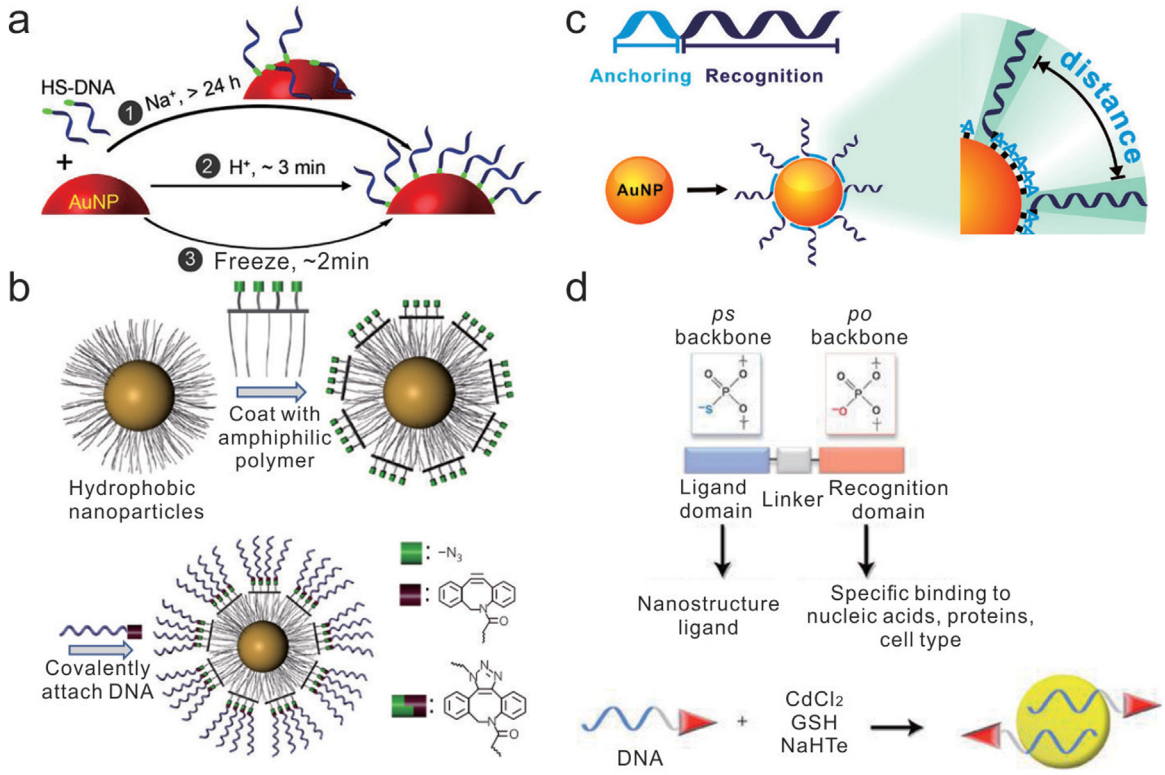

Fig. 3. DNA functionalization of inorganic nanoparticles. a) Attaching ssDNA to AuNPs by (1) salt-aging; (2) low-pH; and (3) freezing. Reprinted with permission from ref. [60] Copyright © 2017, American Chemical Society. b) Functionalization of hydrophobic-capped nanoparticles with DNA through click chemistry. Reprinted with permission from ref. [61] Copyright © 2013, Springer Nature. c) DNA-AuNP conjugates assembling by diblock oligonucleotides. Reprinted with permission from ref [62]. Copyright © 2012, American Chemical Society. d) One-pot synthesis *ps-po*-DNA modified CdTe nanocrystals. Reprinted with permission from ref. [63] Copyright © 2008, Springer Nature.

Besides, nucleic acids with repeated adenines (poly A) and phosphorothioate modifications (*ps*) possess intrinsic affinity for inorganic nanoparticles. As poly A sequences has a high affinity to gold surfaces, Fan et al. developed diblock oligonucleotides without any modification to control the orientation and conformation of the gold surface-tethered oligonucleotides, thereby affecting the hybridization ability of DNA-AuNP conjugates [62]. The diblock sequences contained poly A regions for binding with AuNP and recognition regions for hybridization (Fig. 3c). Nucleic acids with *ps* modifications, which a sulfur atom replaced non-bridging oxygen in the phosphate backbone, possessed affinity for CdTe QDs, because Cd^{2+} showed 3,000-fold higher preference to sulfur than oxygen. In 2009, Kelley et al. developed one-pot strategies for functionalization CdTe crystals with chimeric DNA molecules composed of two domains: one with *ps* modifications served as a ligand to bind with the nanocrystals; the other one with normal phosphodiester backbone (*po*) used for molecular recognition to various targets, such as DNA, proteins and cells [63] (Fig. 3d). Fan et al. reported a purification-free method to control the valency of functionalized QDs [64]. The CdSe/ZnS QDs were pre-modified neutral 2, 5, 8, 11, 14, 17, 20-heptaoxadocosane-22-thiol (mPEG) to form mPEG-QDs. Through incubation with chimeric DNA containing various adenines with *ps* modifications, monovalent, divalent, trivalent and tetravalent QDs were generated with high yield (> 96%, 95%, 80% and 85%, respectively).

Biological molecules

DNA-Protein conjugates combine the recognition ability of DNA and the function of protein, which have great applications in constructing enzyme cascade reactions [65], biosensing [66] and bioimaging [67]. The automatic solid-phase DNA synthesis enables the addition of various chemical groups on oligonucleotides, which helped the specific binding between DNA and proteins.

The most important thing for DNA-protein conjugates is to maintain the function and activity of protein. Nonspecific conjugation adopted the amino, carboxyl, thiol groups in the amino acids [68]. For example, primary amines on the abundant lysine residues often generate amide bond with carboxyl modified DNA. Some homo- or hetero-bifunctional cross-linkers also played important roles in facilitating the conjugation. Cysteine with low abundance possesses thiol group on its side chain, which could react with amino modified oligonucleotides. N-succinimidyl-3-(2-pyridyldithiol) propionate (SPDP) is a crosslinker for amine-to-thiol conjugation via *N*-hydroxysuccinimide (NHS)-ester and pyridyldithiol reactive groups. Yan et al. used SPDP to crosslink proteins with DNA strands [69]. SPDP was first incubated with proteins to allow amine-reactive NHS esters to react with lysine residues of the protein. Then SPDP modified protein conjugated with thiol modified DNA by a disulfide bond exchange of the activated pyridyldithiol group (Fig. 4a). Furthermore, tyrosine and tryptophan with low frequency have plenty aromatic groups for reaction. Fruk et al. prepared DNA-protein conjugates through binding bifunctional linkers onto tyrosine residues [70]. Then, functionalized DNA strands were conjugated with linkers by click reactions. Three bifunctional linkers all contained a cyclic urazole group at one end, and a maleimide, an azide or a cyclooctyne moiety at the other end. The linkers initially reacted with proteins (streptavidin or myoglobin) through the preformed cyclic diazodicarboxamide, then DNA modified by either a thiol, an alkyne or an azide group was conjugated with the linkers. (Fig. 4b). Although the nonspecific conjugation was the most common method, it may generate heterogeneous mixtures in which can block the protein active site, thereby inactivate the conjugates.

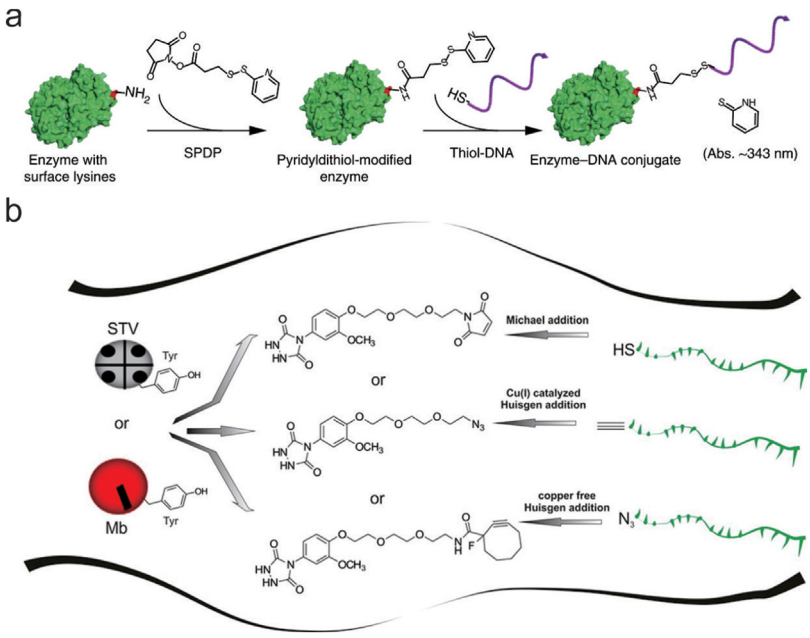

Fig. 4. Covalent conjugation of DNA with protein. a) SPDP chemistry for conjugating thiol modified ssDNA with lysine of an enzyme. Reprinted with permission from ref. [69] Copyright © 2016, Springer Nature. b) Linking thiol, alkyne or azide group modified ssDNA to tyrosine residue of streptavidin or myoglobin. Reprinted with permission from ref [70]. Copyright © 2013, American Chemical Society.

Direct chemical reaction on DNA

Metallization

DNA is an ideal candidate for bottom-up assembled functional nanodevices. However, DNA cannot build such devices independently, due to its poor electric conductivity. Therefore, it is stand to reason that proper metallization of DNA can increase the conductivity while inherit the geometric feature of DNA nanostructures. Moreover, metallization endows DNA with magnetic and optical properties that further broadened its potential applications. In recent years, various metal elements have been explored, such as Au, Ag, Pd, Pt, Co, Cu, and Ni. The DNA metallization process could be generally divided into three stages: 1) Activation. Cationic ions or nanoparticles attach to negatively charged DNA backbones through electrostatic or coordination interaction; 2) Reduction. Reductive agents (chemical agents, ultraviolet light and electricity) transform metal cations into clusters; 3) Growth. The unbounded or newly introduced ions/nanoparticles are further reduced or deposited on the initial metal clusters sites. In general, DNA metallization has three approaches: chemical reduction, electrochemical deposition and photoreduction.

Chemical reduction. Chemical reduction makes use of reagents such as hydroquinone, dimethylamine borane (DMAB), sodium borohydride, alkaline solution and ascorbic acid to help the reducing of metal ions or nanoparticles. In 1998, Braun et al. were the first time to utilize this method to construct silver nanowires on λ-DNA templates [71]. They stretched DNA templates between two gold electrodes, then silver ions condensed along the DNA chain through Ag^+/Na^+ ion exchange. These silver ions were reduced to silver clusters and finally formed conductive nanowires under the help of hydroquinone (Fig. 5a). The resulting nanowire was 12 μm long, 100 nm wide, but had a resistance over 10^{13} Ω. Despite the poor electrical conductivity, this work shed light on the study of DNA metallization. Using the similar chemical deposition technique, Ritcher et al. achieved palladium metallization of DNA in aqueous solution and on glass surface [72]. The conductivity of final nanowire reached 1/10 of bulk palladium. Besides ions, metal nanoparticles can also be used in the "Activation" process. In 2011, Liedl et al. proposed that positive amine modified gold nanoparticles (AuNP) with a diameter of 1.4 nm could bind with DNA origami and serve as seed sites for metallization [73] (Fig. 5b). Recently, after improving the standard electroless process, Porath et al. realized thin and uniform gold nanowires with high conductivity [74]. The inductive AuNP (1.5 nm) was first deposited on DNA molecules under acid condition, then gold ions and reductive ascorbic acid were mixed together to form enhancement solution. Finally, the AuNP-DNA was placed in enhancement solution flow to grow uniform nanowires. The conductive nanowire was 10 nm high, 700 nm long and the resistance was less than 3 kΩ. Apart from electrostatic interaction between ions/nanoparticles and DNA backbones, the reduction could also take place on nucleobases. Ford et al. utilized Pt^{2+} ion to pair with N7 atoms of purine nucleotides [75]. The generated colloidal Pt/DNA showed excellent long-term stability, which could be precursors for the following metallization. Using these precursors, researchers synthesized metal nanowires with multiple compositions, e.g., Au [76], Co [77], Ag [78], Fe [79], Pt [80], Ni [81], Cu [82].

DNA origami has great potential to fabricate nanoelectronic devices with high resolution and large scale. However, there remains several challenges, e.g., maintain the integrity of DNA origami during processing, eliminate disturbance from excess staple strands and realize more accurate metallization. In 2005, Zinchenko et al. fabricated silver nanoring templated by DNA toroid in silver nitrate solution [83]. In this system, Ag^+ ions initially absorbed onto DNA toroid surface through electrostatic interaction, then reduced by sodium borohydride ($NaBH_4$). Harb et al. investigated metallization of branched DNA origami with good selectivity [84]. Briefly, Ag^+ was reacted with aldehyde groups modified on DNA origami, followed by Ag seeding and electroless plating of Au with Ag seeds (Fig. 6a). Both staple strands and ion concentration had significant influence on the template stability and selectivity of metal deposition during this process. This work was a key step toward DNA-templated nanocircuits. In the same year, they also achieved metallization of the same DNA nanostructures by Pd seeding and Au plating method [76]. Recently, this group fabricated continuous metal structures with various shapes on DNA origami [85]. They attached AuNRs on DNA origami, then the nanorod-

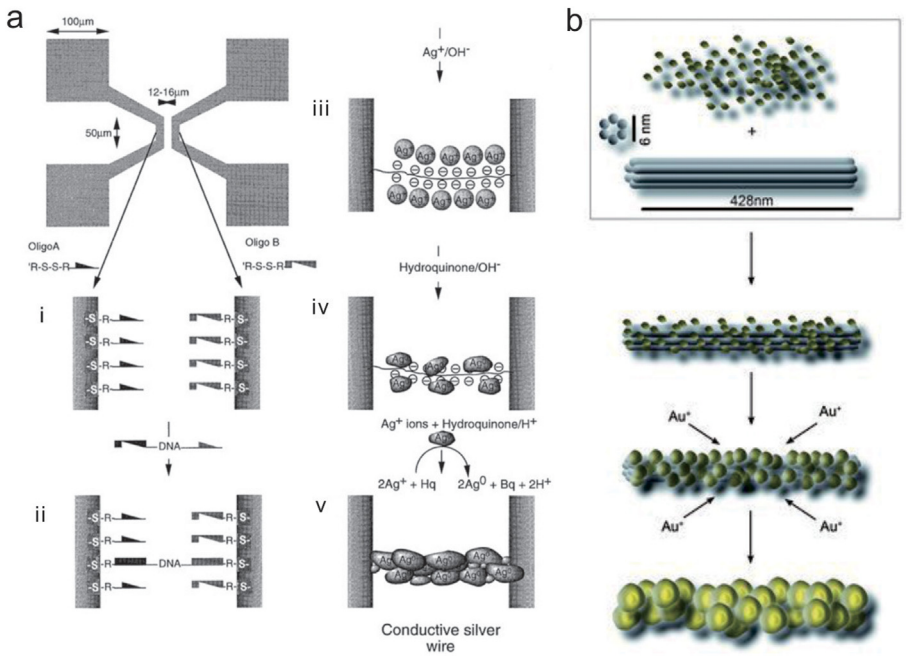

Fig. 5. DNA metallization through chemical reduction. a) Constructing a DNA-templated nanowire between two gold electrodes. Reprinted with permission from ref. [71] Copyright © 1998, Springer Nature. b) DNA origami-templated metallization of positively charged nanoparticles. Reprinted with permission from ref [73]. Copyright © 2011, John Wiley and Sons.

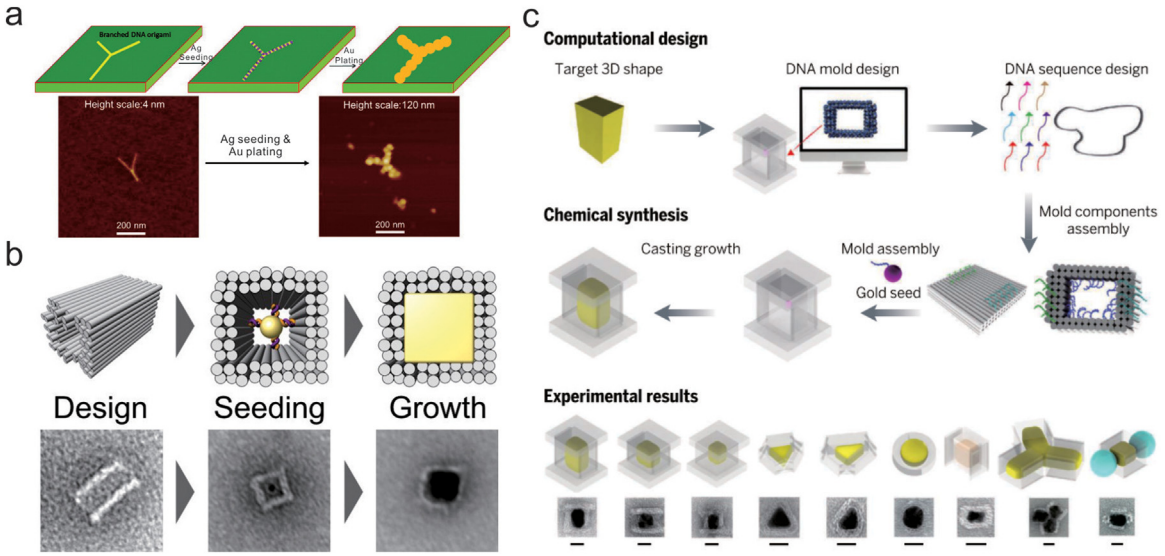

Fig. 6. DNA origami-templated metallization. a) Metallization of branched DNA origami. Reprinted with permission from ref. [84] Copyright © 2011, American Chemical Society. b) Growth of gold nanostructures with programmable shapes in DNA origami harboring an internal cavity. Reprinted with permission from ref [86]. Copyright © 2014, American Chemical Society. c) Casting metal nanoparticles with prescribed shapes within DNA nanostructures molds. Reprinted with permission from ref [87]. Copyright © 2014, The American Association for the Advancement of Science.

seeded origami was undergone electroless gold plating. With the anisotropic growth of nanorods, the gaps between the nanorods would be filled to create continuous structures.

Other than providing inner frameworks, DNA nanostructures with internal cavities could serve as external molds to restrict the growth of metal nanostructures. Seidel et al. put Au seed into a hollow DNA origami mold [86]. After adding hydroxylamine and $H[AuCl_4]$, the synthesized metal nanoparticle was in homogeneous manner. As the mold was open ended, the size of finally obtained nanoparticle was depended on the amount of $H[AuCl_4]$ (Fig. 6b). Yin et al. designed stiff molds with covered lids to effectively confine the metal growth [87]. After enclosing a small nucleating Au seed and reducing process, the Au seed grew into a lager nanometals, which replicated the 3D shapes of molds. As a result, various nanoparticles with 3 nm resolution were fabricated, including Ag and Au nanoparticles with different sizes and shapes, composite structures with homogeneous or heterogeneous components (Fig. 6c).

In the above examples, cations/nanoparticles attached to DNA backbones uniformly, in other words, without selectivity. This will affect the hybridization ability of DNA and related biological applications. Therefore, sequence-selective metallization has attracted much attention. In 2004, Braun et al. introduced reductive aldehyde sites onto DNA backbones through the reaction between

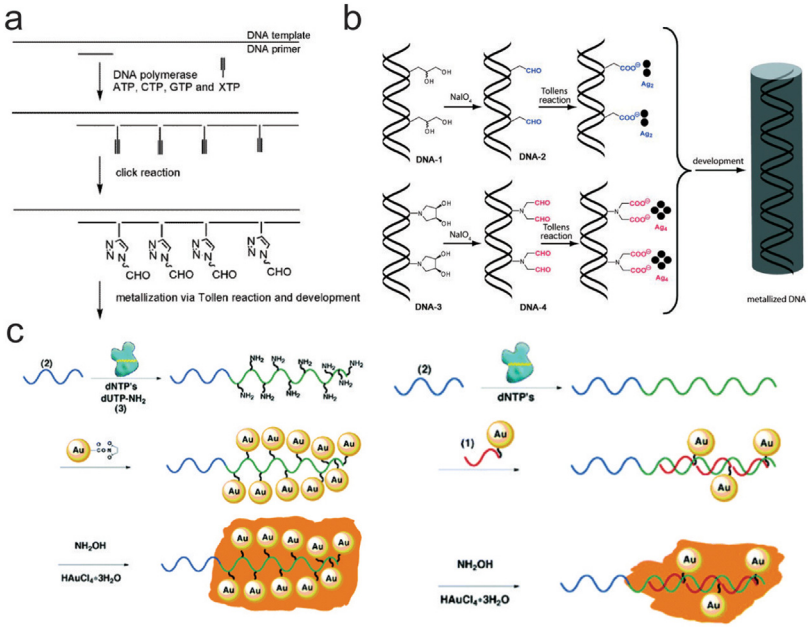

Fig. 7. DNA-templated selective metallization. a) Selective metallization of DNA labelled with aldehyde groups. Reprinted with permission from ref. [89] Copyright © 2006, American Chemical Society. b) Control metallization of aldehyde- and dialdehyde-modified DNA. Reprinted with permission from ref [91]. Copyright © 2009, John Wiley and Sons. c) Metallization of Au nanowires via covalent conjugation of polyamino-functionalization telomer with active-ester-functionalization AuNP or hybridization of ssDNA modified AuNP and telomer, and subsequent catalytic enlargement of AuNPs. Reprinted with permission from ref [94]. Copyright © 2014, American Chemical Society.

glutaraldehyde and primary amine groups on DNA molecules [88]. Subsequent reduction process will only occur on these aldehyde sites. The as prepared Au-DNA nanowires showed a high conductivity (resistivity $\sim 1.5 \times 10^{-7}$ Ωm) and maintained the recognition abilities and biological functionality. Carell et al. adopted an enzymatic method to introduce aldehyde groups selectively [89]. They first introduced acetylene modified pyrimidine nucleotides into target sites during the DNA synthesis. Then aldehyde azides were conjugated to acetylene groups via "click reaction". In this way, selective deposition of Ag cluster around aldehyde-modified DNA was achieved (Fig. 7a). Similarly, they introduced alkyne modified cytosines into DNA [90]. Later on, Carell et al. found out that dialdehyde groups on DNA could reduce Ag^+ ions into Ag_4 cluster and these groups would be more reliable than aldehyde groups (each group reduced two Ag^+ into Ag_2 cluster) in DNA metallization [91]. To construct DNA with dialdehyde groups, DNA was initially functionalized with cis-3,4-dihydroxypyrrolidine, which was then cleaved by sodium periodate to form closely packed dialdehyde groups on DNA (Fig. 7b). Except for the aldehyde groups, Caruthers et al. reported borane moiety in place of the nonbridging oxygen could reduce Au^{3+}, Ag^+ and Pt^{2+} into corresponding metal clusters [92]. Takenaka et al. found Naphthalene diimide-galactose could intercalate selectively into double DNA strands [93]. Subsequently, Ag clusters was formed on the modified sites through silver mirror reaction, which can further grow into Ag-Au core-shell nanowires.

Cationic nanoparticles could also play the role of nucleus for selective metallization. Willner et al. proposed two methods to generate Au nanowires based on telomer templates (the templates contain constant repeat units) [94]. In one method, polyamino-functionalized telomers covalently attached to active-ester-functionalized AuNP, followed by catalytic enlargement AuNPs yielding Au nanowires. In another method, complementary strands modified AuNPs hybridized with telomer repeats, and catalytic enlargement of these AuNPs yielded Au nanowires (Fig. 7c). Harb et al. reported a strategy of selective depositing two different metals to form metal-metal junction on a single DNA origami [95]. In their design, part of the DNA template was firstly metallized by Au with cationic AuNPs as seeds. Then this metallized region served as "chemical mask" to prevent unwanted deposition in the following metallization process.

Chemical reduction is a simple and widely-used method. Both homogeneous and selective metallization could generate high conductive metal nanostructures. Specially, selective metallization maintains the biological functionality of DNA and reduces the background. However, the reducing agents may contaminate, denature or destruct the DNA scaffold via chemical attack.

Electrochemical metallization. Electrochemical metallization contains an electron transfer process from substrates to metal ions with the help of working electrode. In 2007, Yang et al. first reported this method to prepare silver nanowires on DNA templates [96]. The Au substrate electrode was exposed to DNA solution, then immersed into Ag^+ solution for a time scale for activation, which step was important for the formation of nanowires. The reduction of Ag^+ was performed by Bulk Electrolysis with Coulometry (BE). There are many influencing parameters of the resulting nanowires: the number of activation times and electrolytic times affected the sizes and shapes of nanowires; the concentration of Ag^+ and electrolytic time controlled the diameters of nanowires; the length of DNA templates determined the length of nanowires. Jayaraman et al. reported electrochemical synthesis of metal-DNA (M: DNA) nanohybrids [97]. They first prepared M^{n+}: DNA complex, then the complex was coated on conductive substrates via layer-by-layer deposition, drop-casting or electrostatic deposition. At last electrons were transferred from pyrolytic graphite (HOPG) substrates to metal ions attached to DNA. Houlton et al. fabricated magnetic nanowires through electrochemical method [98] (Fig. 8). In this process, n-doped Si<100> wafer served as working electrode because it has been verified that n-type silicon could provide electrons for silver reduction [99]. The process contains two stages: Fe^{2+} ions first hybridized with DNA templates for activation, then they were reduced to zerovalent Fe on the working electrode.

Currently, using electrochemical metallization method, the sizes and shapes of DNA-metal complex can be well-tuned by vary-

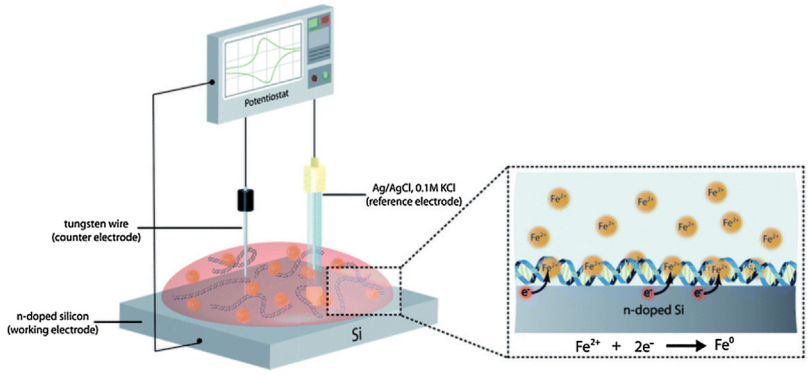

Fig. 8. DNA-templated Fe nanowires produced by electrochemical approach. Reprinted with permission from ref. [98] Copyright © 2013, Royal Society of Chemistry.

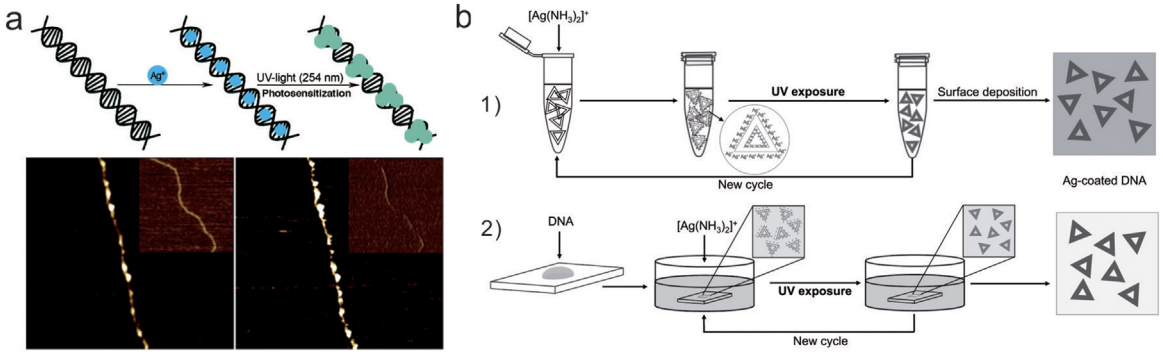

Fig. 9. DNA metallization through photochemical reduction. a) Photoinduced silver deposition on DNA templates. Reprinted with permission from ref. [100] Copyright © 2005, American Chemical Society. b) Photochemical reduction for silver coating of DNA origami using (1) solution route or (2) surface route. Reprinted with permission from ref [102]. Copyright © 2018, IOP Publishing.

ing electrochemical parameters such as potential and electrolysis time. However, selective metallization remains challenging.

Photochemical metallization. Photochemical metallization refers to the reduction process induced by UV irradiation. In 2005, Berti et al. first fabricated silver nanowires through DNA-templated photoreduction of silver ions [100]. The DNA-Ag^+ helix was exposed to 254 nm UV light, and the characteristic adsorption peak at 420 nm represented the generating of Ag nanoparticles for their surface plasmon resonance. This complexation/photoreduction cycle was repeated for four times to increase the number and polydispersity of Ag nanoparticles. They found the metal growth occurred exclusively along the DNA chain (Fig. 9a). The possible mechanism is that DNA itself acted as photosensitizers in this process, as the short-wavelength UV irradiation caused photooxidation of DNA bases. Both reactive radical intermediates and singlet oxygen generated in the photooxidation would play a role in the reduction of metal ions. However, disagreed with Berti, Murata et al. claimed that the reduction agents (such as alcohol) in silver ion solutions were necessary for photochemical reduction [101]. The free radicals during abstraction of α-hydrogen from alcohol molecules would reduce silver ions into DNA-metal nanocomposites. Very recently, Hillier et al. realized silver metallization on DNA origami through photochemical route [102]. In their design, triangular DNA origami could drive silver metal formation by UV exposure. The DNA strands were photosensitizer to reduce silver ions directly on DNA origami surface. This system could work with a high yield both in solution and on solid surface (Fig. 9b).

Although the mechanism is not thoroughly understood, photochemical metallization is undoubtedly a promising method. So far, this method has been achieved in metallization of Au [103], Ni/Co [104], Pt [105] and Au-Ag nanoalloy [106] metallization. Similar to electrochemical method, at present, it is difficult to achieve selective metallization through photochemical metallization.

Mineralization

Compared to metallization, mineralization of DNA occurs in nature [107,108] and can be further tuned by DNA nanotechnology. DNA mineralization utilizes DNA and self-assembled DNA nanostructures as "organic" templates to form well-designed "inorganic" materials, such as DNA-silica composites with nanoscale accuracy. In return, mineral shells enhance the chemical and mechanical stabilities of DNA nanostructures.

A critical issue in DNA mineralization is to achieve effective mineralization source attachments onto DNA, either ions or molecules. For example, the common method of DNA silicification is to use positively charged inorganic precursors that electrostatically interact with negatively charged DNA backbones. However, the silica species carry negative charges under pH 4.3–11.9, the range that negatively charged DNA molecules could maintain their double-helix configuration. Hence, the combination of silica species and DNA would be hindered. The most effective solution is to introduce a cationic inducting molecule attaching on DNA to absorb the anionic silica species.

In 2004, Shinkai et al. tried to use DNA helix as template to guide silica mineralization [109]. They designed a molecule which had two guanidinium heads to form an ion pair with phosphate backbone of DNA molecule, and an ammonium tail to interact with silica species (Fig. 10a). During mineralization, DNA was premixed with cationic didodecyldimethy-lammonium bromide (DMAB) to increase its solubility in organic solutions, since the mineralization source tetraethoxysilane (TEOS) is dissolved in organic solvent. Then the guanidinium heads attached to DNA backbones via cation-exchange with DMAB. At last the ammo-

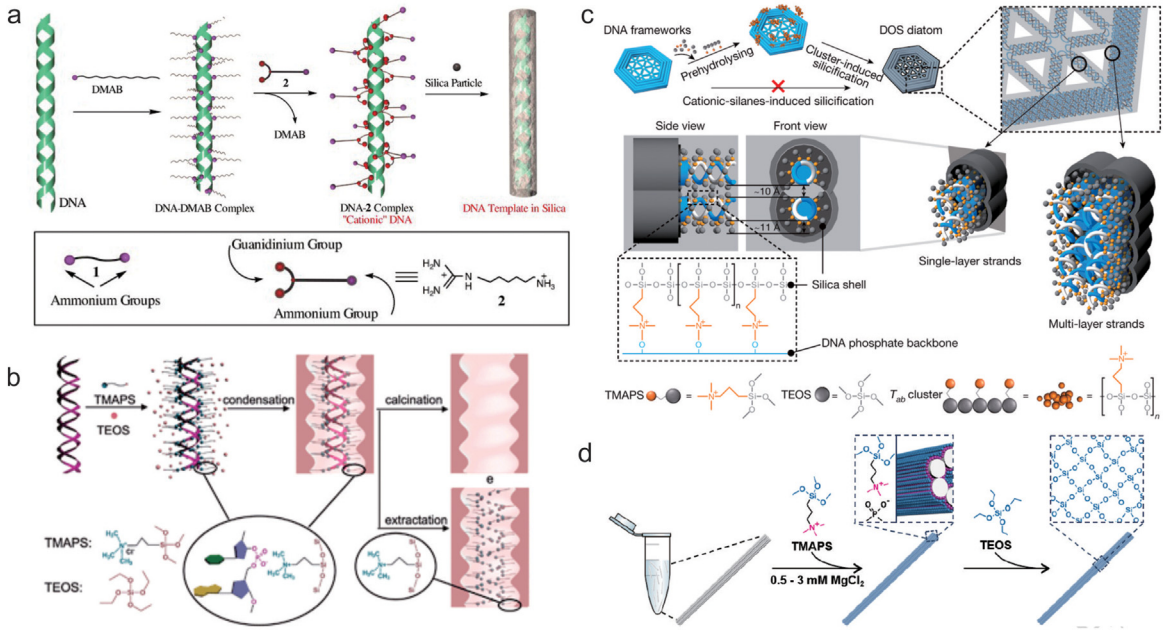

Fig. 10. Current methods of DNA-templated mineralization. a) DNA-templated silicification with Sol-Gel reaction. Reprinted with permission from ref. [109] Copyright © 2004, John Wiley and Sons. b) Transcription of DNA into porous silica by co-structure directing route. Reprinted with permission from ref [110]. Copyright © 2009, Royal Society of Chemistry. c) DNA origami-templated silicification via mixing DNA origami with prehydrolysed TMAPS and TEOS. Reprinted with permission from ref [113]. Copyright © 2018, Springer Nature. d) DNA origami silica encapsulation in low cationic solutions. Reprinted with permission from ref. [114] Copyright © 2018, John Wiley and Sons.

nium group on "cationic" DNA were used for further deposition of TEOS. Che et al. transcribed DNA into mesoporous silica through a co-structure directing route [110]. N-trimethoxyl-silylpropyl-N, N, N-trimethylammonium chloride (TMAPS) was used as co-structure directing agent (CSDA), which contained positively charged quaternary ammonium head to interact with DNA backbones and alkoxysilane sites could co-condense with TEOS to form DNA templated silica fibers (Fig. 10b). In a following work, they synthesized DNA-silica complex (DSC) with 2D square *p4mm* structure, 2D hexagonal *p6mm* structure and their mixtures by adjusting DNA concentration [111]. Further combining DNA chiral assembly and silica mineralization, they produced 3D impeller-like chiral DNA-silica assemblies [112]. In 2018, Fan et al. established DNA origami silicification (DOS) method to solve the problem that TMAPS could hardly combine with DNA nanostructures under high magnesium concentrations [113]. In their design, pre-hydrolyzed small clusters of TMAPS and TEOS with stronger positive charges could better compete with magnesium ions. (Fig. 10c). With this approach, complex DNA-silica composites expanding from 2D to 3D were precisely prepared. The nanomechanical property of the composites was ten times higher than bare DNA templates, while maintained good flexibility. Very recently, Jungemann et al. realized silica mineralization of individual DNA origami and large 3D DNA crystals in solution [114] (Fig. 10d). Certain DNA origami was found stable in low cationic solutions (e.g., 0.5∼3 mM $MgCl_2$), and TMAPS seems to be able to compete with magnesium ions at this low concentration. This phenomenon is very interesting, since the charge density of a single TMAPS molecule is far less than divalent magnesium, and there is no direct evidence that TMPAS could firmly wrap around DNA origami. They also found liquid disturbance would prevent silica mineralization, thus a 7-day's undisturbed state was necessary for single DNA origami structures. For larger crystal structures, the mineralization time extended up to 9 days. The field of DNA nanostructure mineralization is just getting started, and many issues remain to be explored, e.g., understanding the mineralization mechanism, expanding the mineral type and realizing applications (Table 1).

Polymer coating

Nucleic acids, including plasmid DNA and antisense oligodeoxyribonucleotides (ODN) have attracted much interest for their potential in gene therapy [115]. DNA-based nanodevices also have great potential in nanomedicine and molecular biology applications [116,117]. However, DNA nanostructures will be deformed in cell culture buffers or biological fluids with a low ionic strength, and nucleic acids would suffer from severe enzymatic digestion by nucleases in physiological environment. Polymers coated on DNA nanostructures can protect DNA from degradation and maintain their conformations and functions at the same time.

Electrostatic interaction. Polycations can wrap DNA nanostructures and form polyplex micelles through electrostatic interaction. Kataoka et al. conjugated poly (ethylene glycol)-poly (L-lysine) (PEG-PLL) AB-type block copolymers with plasmid DNA [118]. They found the cationic PLL segment could interact with DNA effectively, the outward PEG segment would maintain the stability of complex. Compartmentalization of DNA structure into PEG environment enhanced DNA stability, as demonstrated by the increased resistance against DNase I. Schmidt et al. encapsulated various DNA origami into this block copolymer [119]. The polyplexed DNA origamis were stable under the digestion of DNase I and fetal bovine serum (FBS), as well as low salt concentrations. Moreover, functional molecules and materials could attach to the DNA nanostructures after the protection. At the same year, Shih et al. found that DNA origami coated with oligolysine-PEG (K_{10}-PEG) copolymers exhibit a 1000-fold anti-digestion ability against serum nucleases, which was much higher than bare oligolysine coating [120]. This K_{10}-PEG-stabilized DNA nanostructures exhibited good intracellular integrity and increased pharmacokinetic bioavailability in mouse model (Fig. 11a). Compared with PLL, cationic poly (2-dimethylaminoethyl methacrylate) (PDMAEMA) possessed higher transfection efficiency. In a work proposed by Kostiainen et al., the homopolymer PDMAEMA, AB-type PDMAEMA-PEG and ABA-type PDMAEMA-PEG-PDMAEMA block copolymers were developed [121]. Among them, PEG moi-

Table 1
Major routes of large-scale DNA nanostructures.

Routes	Examples	Size
Stick-end cohesion	24 helices × 28 helical turns (24H × 28 T) rectangles assemble from single-stranded tiles [29]	64 nm × 103 nm
	12H × 177 T tubes [29]	31.2 nm × 619.5 nm
	1D chains assembled from Z-shaped tiles [32]	several microns in length
	Rhombus shaped single-stranded origami [26]	250 nm in edge
	Hexagonal 2D DNA array assembled from three-point-star motifs [38]	1 mm in dimension
	2D arrays assembled from six-point-star motifs [36]	40 μm in dimension
	10 × 10 DNA origami arrays [39]	880 nm × 880 nm
	Fractal assembled 8 × 8 DNA origami arrays [30]	704 nm × 704 nm
	2D tiles or tubes assembled from DNA-origami hexagon tiles [35]	Hundreds of nanometers to micron in length
	Molecular canvas assembled from 32-base DNA bricks [20]	25 nm × 25 nm × 27 nm
	3D nanostructures assembled from 52-base DNA bricks [24]	100 nm × 100 nm × 100 nm
	3D DNA crystals assembled from tensegrity triangles [37]	Up to 250 μm in dimension
	3D DNA crystals assembled with layered-crossover tiles [40]	Up to hundreds of micrometers in dimension
	3D hexagonal DNA crystals [41]	50-200 μm in dimension
	Blunt-end stacked DNA origami [33]	4 μm in length
	2D lattices made from cross-shaped DNA origami tiles [34]	6 μm in length, 1~3 μm in width
Base-pair stacking	Lipid-bilayer-assisted 2D DNA origami structures [31]	1.2 μm × 1.2 μm
	Tube-like structures assembled from V bricks [28]	more than 1 μm in length, several hundred nanometers in diameters
	3D polyhedral [28]	220 nm in radius
	3D rhombohedral polycrystalline [42]	up to 2.5 μm^2

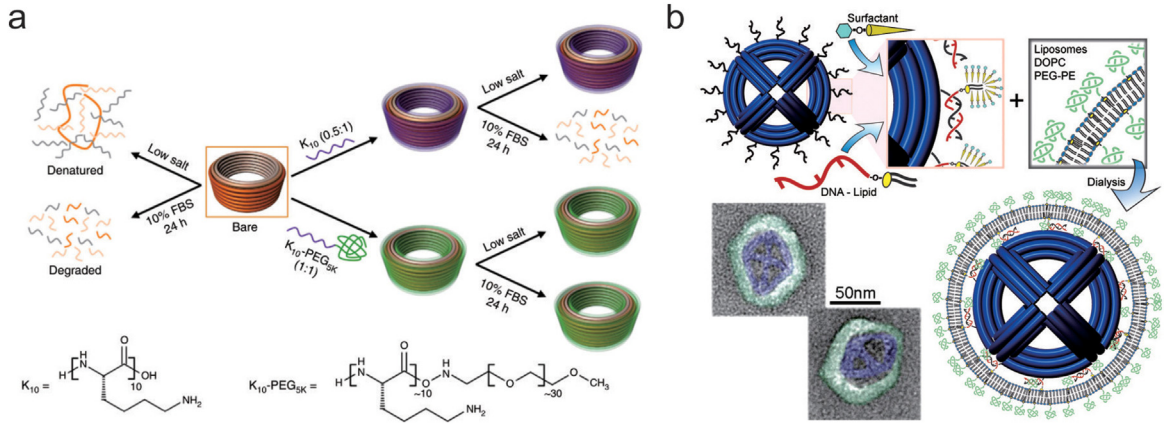

Fig. 11. Methods of DNA-origami templated polymer coating. a) DNA origami coated with PEG-K_{10} block copolymers to enhance stability. Reprinted with permission from ref. [120] Copyright © 2017, Springer Nature. b) DNA origami encapsulation in lipid bilayers. Reprinted with permission from ref [122]. Copyright © 2014, American Chemical Society.

eties provided the protective features and ABA-type achieved the most efficient binding with DNA structures. The nontoxic polymer coating may improve the transfection rate of DNA origami and enhance the stability of origami in biological environments.

DNA hybridization. Single oligonucleotides modified with polymers could serve as protective agents for DNA nanostructures through hybridization. Shih et al. encapsulated DNA nano-octahedron (DNO) into lipid bilayers [122]. The lipid-conjugated oligonucleotides were preassembled to the DNO surface in a surfactant solution. After adding liposomes, surfactant-lipid micelles were formed. A dialysis process was used to remove the surfactant and achieve fused lipid bilayer around the DNO eventually (Fig. 11b). Compared to bare DNA nanostructures, encapsulation of DNA nanostructures into lipid bilayers could enhance protection against nuclease digestion, decrease immune activation and improve pharmacokinetic bioavailability.

Pattern transfer from DNA

Pattern transfer is a process that the shape of a template is inherited a substrate. In a typical pattern transfer process, a patterned resist layer is used to block the etchant from reacting with the underlying substrate. The self-assembled DNA nanostructures can be excellent candidates as they provide a variety of templates with high spatial resolution. With patterned substrates, the locations and orientations of DNA nanostructures are precisely controlled. After patterned DNA nanostructures on substrates, these nanostructures could be utilized as etch masks to transfer their nanoscale structural information to the substrates, such as silicon dioxide and graphene. Two critical factors need to be considered in this process: one is maintaining the chemical and mechanical stability of DNA nanostructures; the other is improving the adhesion efficiency of DNA nanostructures onto the substrates.

Chemical etching

In a work proposed by Liu et al., they found DNA could be used as templates to promote/inhibit the etching of SiO_2 by HF vapor according to different humidity, which resulted in negative/positive tone pattern transfer from DNA to SiO_2 [123]. Previous studies showed that SiO_2 and HF gas react to produce SiF_4 and H_2O, as shown in Eq. (1):

$$SiO_2(s) + 4HF(g) \rightarrow SiF_4(g) + 2H_2O(g) \quad (1)$$

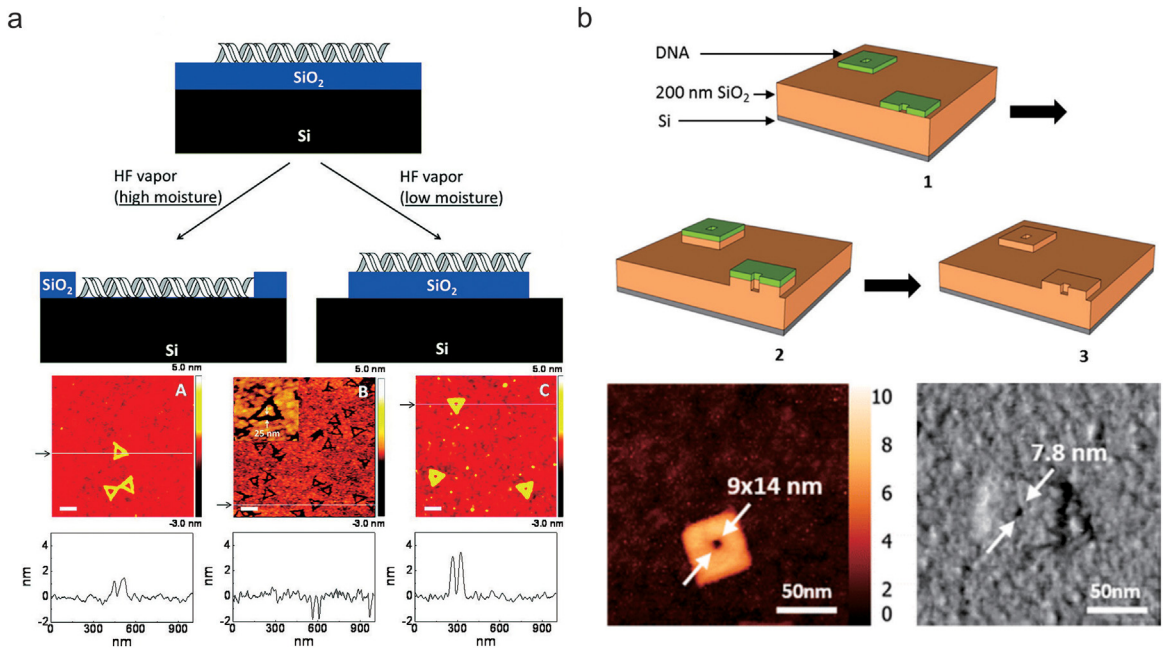

Fig. 12. Pattern transfer through chemical etching. a) DNA-mediated etching and masking of SiO_2 at high or low moisture. Reprinted with permission from ref. [123] Copyright © 2011, American Chemical Society. b) Pattern transfer from DNA origami to SiO_2: 1. Absorption of DNA origami to SiO2. 2. HF vapor etching. 3.Removing the DNA mask and revealing SiO2 patterns. Reprinted with permission from ref. [125] Copyright © 2016, American Chemical Society.

Or (2):

$$6HF + 3H_2O \rightarrow 3HF_2^- + 3H_3O^+$$

$$SiO_2 + 3HF_2^- + 3H_3O^+ \rightarrow SiF_4 + 2HF + 5H_2O \quad (2)$$

The etching rate correlates with the concentration of catalytic water. Thus, when the environment reached high moisture (~50%), water preferred to be absorbed on DNA molecules and resulted in an increase of SiO_2 etching rate, namely negative pattern transfer. On the contrary, SiO_2 retained a monolayer of water at low humidity (~34%). Then the etching rate was decreased, which lead to positive pattern transfer (Fig. 12a). A typical etching time is 5/15 min when DNA functioned as catalyst or protective mask. They also optimized the etching conditions, including reaction temperature, reaction time, HF and water pressure, to produce high-resolution (~10 nm) and high-contrast (>10 nm) pattern transfer to SiO_2. Further, the obtained SiO_2 patterns could be used as hard masks for plasma etching of Si substrates with sub-20 nm features [124].

Tiron et al. used alcohol vapor (A) to realize ionization of HF vapor, which could achieve sub-10-nanometer lithography on SiO_2 substrates [125], as shown in Eq. (3):

$$2HF(ads) + A(ads) \rightarrow HF_2^-(ads) + AH^+(ads)$$
$$SiO_2(s) + 2HF_2^-(ads) + 2AH^+(ads) \rightarrow SiF_4(ads) + 2H_2O(ads) + 2A(ads) \quad (3)$$

The water laying on surface was a product generated by this reaction, and it was also the catalyst of the reaction. Through reducing water by heating (anhydrous HF vapor etching), DNA behaves as negative resist to protect the underlying SiO_2 from etching. In this way, the diffusion of etchant was limited, which leading to sub-10 nm accurate etching (Fig. 12b).

Plasma etching

Plasma reactive ion etching (RIE) removes the unprotected region of the substrates, then the shape information of DNA nanostructures is transferred to the final etched products. The stability of DNA origami is the main concern during this process. Hong et al. proposed that highly oriented DNA nanowires without any modification could serve as etching resist to create graphene nanoribbons (GNRs) [126]. Highly aligned DNA nanowires on graphene substrates were served as masks during etching with oxygen plasma. After removing DNA masks, GNRs arrays could be obtained for further fabricating GNR transistors and two terminal devices. During the carbonization of DNA nanostructures, Liu et al. coated Al_2O_3 film on DNA nanostructures to preserve their shapes at 800–1000 °C [127]. Strano et al. proposed a method of transferring metallized DNA nanostructures to graphene with O_2 plasma etching [128]. They believed unprotected DNA masks would be degraded under plasma, Au metallization of DNA nanostructures provided chemical and mechanical stability that could largely preserve their shape information during etching. Monolayer graphene sheets were firstly grown on copper foils and transferred to SiO_2/Si wafers. Then 1-pyrenemethylamine molecules were pre-adsorbed on graphene to improve the adhesion and dispersion of negatively charged hydrophilic DNA on graphene. After metallization, plasma beam scattering the edges of metallized mask, which could shrink the graphene edges and leave mask-covered regions on wafer. At last, the metallized masks were removed to expose final graphene structures (Fig. 13a). Toppari et al. transferred the spatial information of DNA nanostructures to metal nanostructures through DNA-assisted lithography [129]. First, a silicon layer was grown on Al_2O_3/Si_3N_4 substrate, and DNA origami was deposited on the silicon (step 1–3). After that, a silicon dioxide layer was selectively grown on the top of the bare areas of silicon and slightly on DNA origami (step 4). Then the silicon under the origami was etched by RIE (step 5). Finally, a metal layer was deposited on the whole chip, after removing process, DNA origami-shaped metal nanostructures were left on the substrate (step 6–8) (Fig. 13b). Four types of plasmonic nanostructures (including Seeman tile - ST, bowtie origami - BO and two versions of chiral double L - CDL) were fabricated.

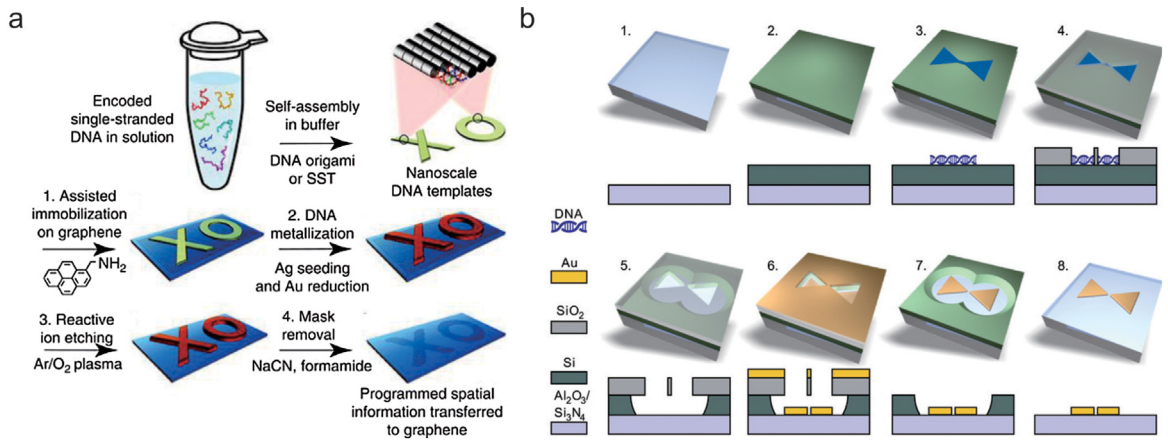

Fig. 13. Pattern transfer with Plasma etching. a) Metallized DNA nanostructures as plasma etching resist for graphene nanopatterning. Reprinted with permission from ref. [128] Copyright © 2013, Springer Nature. b) Step-by-step fabrication procedure of the DNA-assisted lithography method. Reprinted with permission from ref [129]. Copyright © 2018, The American Association for the Advancement of Science.

Lithography combined with DNA nanotechnology

DNA origami nanostructures have great potential for bottom-up fabrication of both biological and electronical nanodevices. However, precise control over the positions and orientations of these solution phase units is difficult, which hinder further application of DNA origami guided nanomaterials. Combination of lithography and DNA nanotechnology has been demonstrated as an effective route to solve this problem.

Noncovalent interactions

Noncovalent interactions, such as electrostatic and hydrophilic interactions, allow DNA origami to dynamically tune their arrangement on the substrate. In 2007, Yan et al. constructed highly ordered DNA nanotube arrays using this strategy [130]. The polydimethylsiloxane (PDMS) stamps were initially patterned by soft lithography. Then DNA nanotubes were aligned into arrays with the help of molecular-combing effect of a directional flow. The DNA nanotube arrays could guide patterned assembly of target species via biotin-streptavidin or DNA hybridization interaction (Fig. 14a). Soh et al. came up with a charge-to-charge strategy to attract and immobilize rectangular origami onto gold surfaces using a carboxylic acid-terminated self-assembled monolayer (SAM) [131]. After polishing, the gold surface was functionalized with 11-mercaptoundecanoic acid (MUA). The carboxylic acid groups of MUA could concentrate and chelate Mg^{2+} ions. These positive ions eventually created a salt bridge between negatively charged DNA origami and gold surfaces. In 2016, according to the report from Rothemund, the self-assembly of DNA origami on lithographically patterned binding sites allowed coupling molecular emitters to photonic crystal cavities (PCC) [132]. In their work, PCCs were fabricated on SiN layer by electron beam, leaving negatively charged carboxylate groups to bind DNA origami via Mg^{2+} ions from the solution (Fig. 14b). In a work reported by Wallraff et al., triangular DNA origami could assemble on hydrophilic oxide regions with high selectivity and good orientation [133]. A trimethylsilyl (TMS) monolayer with regions exposed to O_2 plasma or UV-ozone become hydrophilic for binding of DNA origami; whereas the untreated regions remained hydrophobic and prevented the attachment of origami (Fig. 14c).

Covalent interactions

To achieve better chemical selectivity between substrates and DNA origami, and fabricate more complex nanodevices, covalent interactions (especially Au-S bonding) provide stronger binding forces and higher selectivity for DNA origami patterning on substrates. In 2008, Kuzyk et al. developed dielectrophoretic trapping of single DNA origami between gold electrodes [134]. Electrodes with gaps of 70–90 nm were set on a substrate. DNA origami with appropriate size and thiol groups modified in the middle of each side of the origami would bound to the electrodes through Au-S bonds. However, the trapping rate of a single origami was about 10%, and the rectangular origami were always folded. Yan et al. fabricated gold islands on substrates by electron beam lithography (EBL) to interconnect DNA origami nanotubes [135] (Fig. 15a). In their design, DNA nanotubes with fixed length and thiol groups near both ends could connect the surface patterned gold islands. With four thiol groups at both ends, the yield of gold islands connected by a single nanotube was about 86%. Eritja et al. developed DNA-origami-driven lithography for covalently patterning DNA on gold surfaces, with a resolution of sub-10 nm [136]. In their design, DNA origami containing 12 thiol modified DNA ink staples were assembled and stamped on gold surfaces with the help of Mg^{2+} in the buffer. Meanwhile, Au-S bonds formed between thiol-modified staples and gold surfaces. Then DNA origami was denatured to remove the origami frame, i.e. unmasking step, leaving DNA ink strands bound on the surfaces. Lastly, this DNA pattern could bind with gold nanoparticles that conjugated with thiol oligonucleotides (Fig. 15b). This design exploited DNA origami programmability and DNA lithography to immobilize DNA nanopatterns on surfaces, which took the opportunity for functionalizing and patterning of surfaces for creation of metamaterials in nanoelectronics and photonics field. Rothemund et al. covalently immobilized amino-functionalized DNA origami arrays on Si/SiO_2 surface [137]. The surface was activated by either cyanylating (CDAP) or carboxylating (CTES) agents for crosslinking. Subsequent crosslinking reaction was either spontaneous (CDAP) or catalyst-assisted (CTES) steps using carbodiimide (EDC) and *N*-hydroxysulfosuccinimide (sulfo-NHS) agents (Fig. 15c).

Current applications

The self-assembled DNA origami nanostructures display 5 nm-resolution for binding sites. Thus, nanomaterials can be positioned on the structures with high accuracy. Variety of applications are associated with compact arrangements of materials, such as inorganic materials and enzymes. On one hand, surface plasmon properties are closely related to the arrangements, composition and shape of materials, including properties of chirality, Surface-Enhanced Raman Spectroscopy (SERS) and fluorescence. DNA

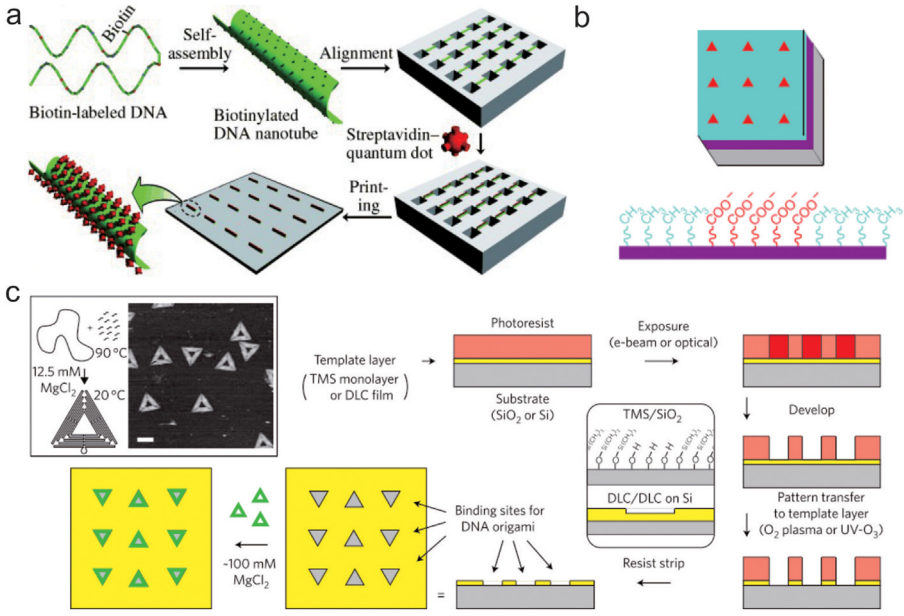

Fig. 14. DNA lithography with noncovalent interactions. a) Alignment of DNA nanotube arrays. Reprinted with permission from ref. [130] Copyright © 2007, John Wiley and Sons. b) Fabrication of a single binding site for DNA origami mediated by cationic ions. Reprinted with permission from ref [132]. Copyright © 2016, Springer Nature. c) Placement of individual DNA origami through hydrophilic interactions. Reprinted with permission from ref [133]. Copyright © 2009, Springer Nature.

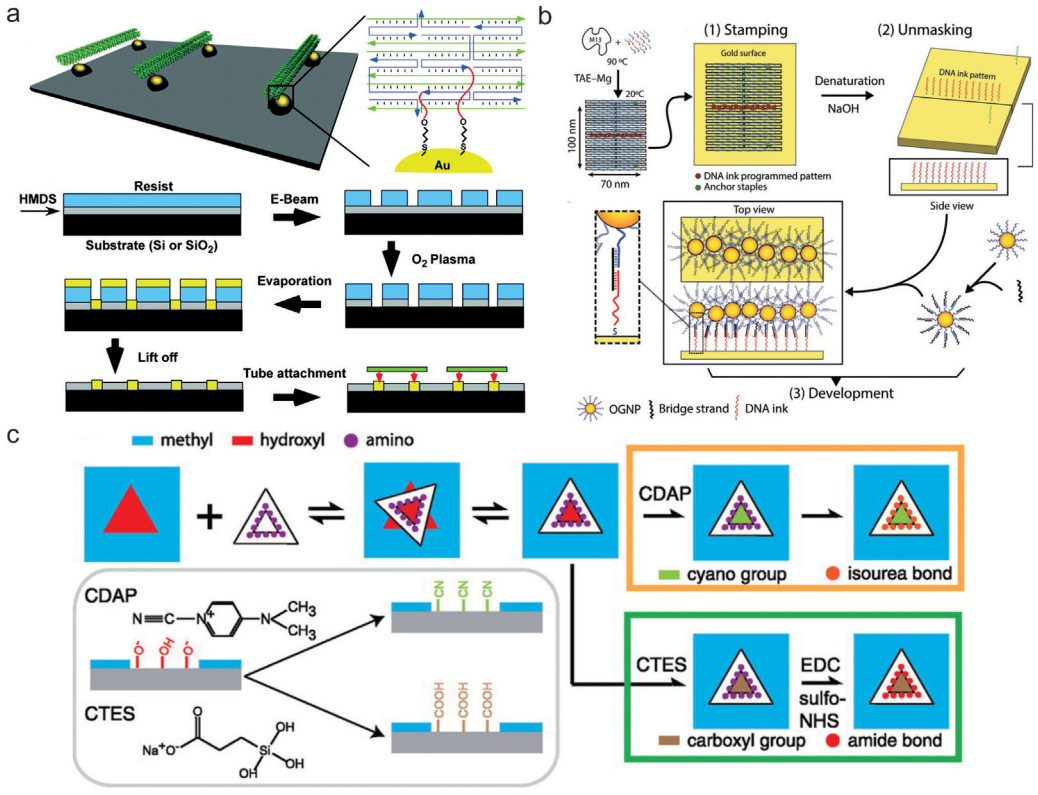

Fig. 15. DNA lithography with noncovalent interactions. a) DNA nanotubes interconnected by gold islands. Reprinted with permission from ref. [135] Copyright © 2010, American Chemical Society. b) Covalently transferring DNA origami information to the gold surface. Reprinted with permission from ref [136]. Copyright © 2017, John Wiley and Sons. c) Covalent coupling single DNA origami nanoarrays on Si/SiO_2 substrates. Reprinted with permission from ref. [137] Copyright © 2014, American Chemical Society.

nanostructures would help to fabricate the required plasmonic nanostructures with these materials, yielding enhancement of surface plasmon properties. On the other hand, the spatial and temporal arrangement of enzymes into well-defined complexes leads to enhanced activity. The ability to mimic these complexes through fabrication with DNA nanostructures is a useful tool for constructing more efficient enzymatic nanoreactors than native systems.

Chiral plasmonic enhancement

Circular dichroism is observed when optically active material absorbs left-handed and right-handed polarized light slightly differently. It is a common technique to study chiral molecules which are not coincident with their mirrors by simple rotation and translation. Chiral molecules are widely found in nature, for example,

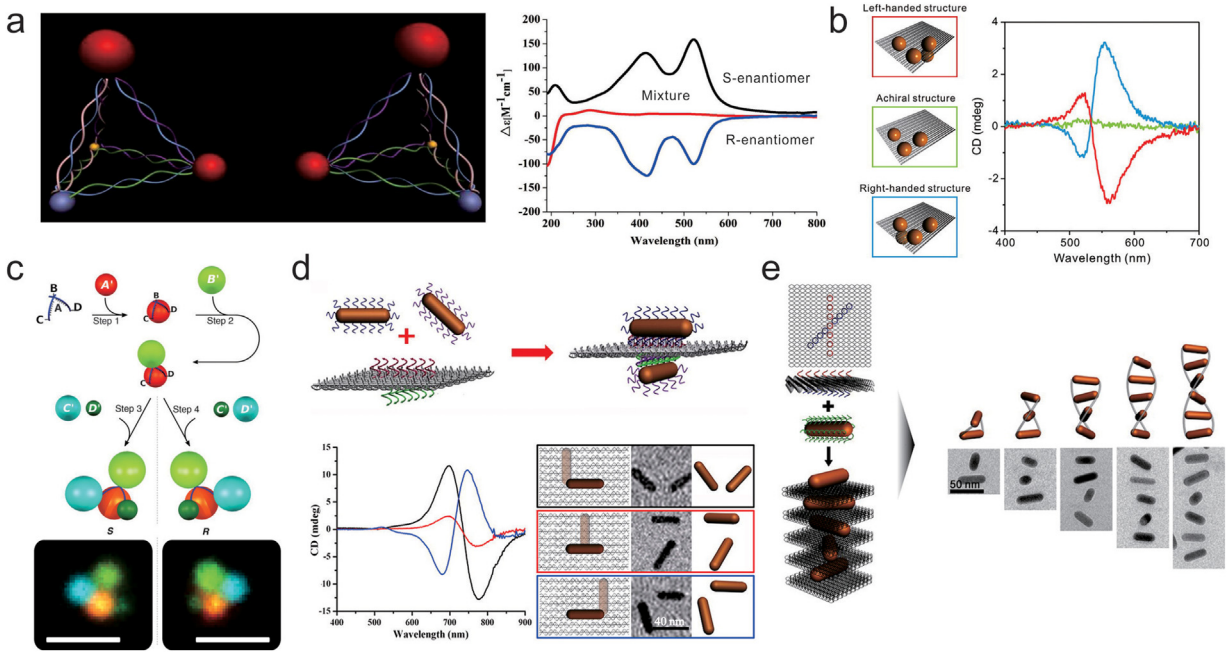

Fig. 16. Chiral plasmonic enhancement through ssDNA- and DNA origami-nanoparticle hybrids. a) Chiral nanoparticle pyramids made from DNA-nanoparticle hybrids with strong R/S optical activity. Reprinted with permission from ref. [139] Copyright © 2012, American Chemical Society. b) 3D plasmonic chiral AuNP tetramers assembled by DNA origami. Reprinted with permission from ref [140]. Copyright © 2013, American Chemical Society. c) 3D chiral colloidal architectures constructing by DNA origami L belt. Reprinted with permission from ref [142]. Copyright © 2017, The American Association for the Advancement of Science. d) 3D anisotropic AuNR dimers forming by using bifacial DNA origami as templates. Reprinted with permission from ref [143]. Copyright © 2013, American Chemical Society. e) Self-assembly of right handed-AuNR helices. Reprinted with permission from ref [144]. Copyright © 2015, American Chemical Society.

proteins and DNA showing weak CD in ultraviolet (UV) region. But the weak chiroptical activity and the limitation in UV range hindered their applications. Thus, chiral enhancement is necessary in the construction of polarized materials, preparation and separation of chiral biological molecules and chiral drug molecules. Chiral nanomaterials assembled by DNA are of particular interest. Alivisatos et al. firstly used four ssDNA-AuNP conjugates to create chiral pyramids with AuNPs (5, 10, 15 and 20 nm) at the tips [138]. *S* and *R* enantiomers were constructed through switching 5 and 10 nm particles. However, no obvious optical properties were found of these chiral nanostructures because of the instable configuration and large distance between neighboring nanoparticles (≥8 nm). Kotov et al. assembled chiral pyramids containing metal and/or semiconductor nanoparticles with a yield of 80% [139]. The self-assembled pyramids made from 15 nm AuNP + 25 nm AuNP + AgNP + QDs showed strong CD activity, with anisotropy *g*-factors as high as 1.9×10^{-2} in visible light region (Fig. 16a).

The rigid and addressable DNA origami realize precise organization of four nanoparticles into 3D asymmetric tetramer. With protruding capture strands from four binding sites, Ding et al. organized four AuNPs (20 nm) on rectangular bifacial DNA origami [140]. As three of four binding sites were placed on one side, four AuNPs could be arranged in left- and right-handed nanostructures through DNA hybridization. The resulted structures presented characteristic bisignate CD response, which confirmed the isotropic nature of these structures (Fig. 16b). Based on this work, Wang et al. systematically tuned the particle size and interparticle distance of the AuNPs tetrahedron to engineer the chiral optical properties [141]. They found that increasing the interparticle distance and decreasing the particle size would weaken the CD signal. Chaikin et al. extended the nanometric scale into micron-sized colloidal clusters by conjugating DNA origami with colloidal particles [142]. A DNA origami L belt combined with four colloids of various sizes, one polymethyl methacrylate colloid (PMMA, 0.71 μm) at central and three polystyrene colloids (PS, 0.8, 0.69, 0.4 μm separately) pointed away from central one, which formed satellite structures. Using confocal microscopy, *R*- and *S*- enantiomer could be observed (Fig. 16c).

Although spherical nanoparticles have been successfully employed in constructing plasmonic structures, nanorods showed more distinct advantage: 1) two nanorods with certain angles can generate chiral activity, while discrete and rationally designed plasmonic nanostructures were hard to realize by four spherical nanoparticles; 2) The nanorods exhibit lateral plasma resonance comparable to spherical nanoparticles, and distinct longitudinal plasma resonance, thus a small angle between nanorod dimers would cause strong CD response. Wang et al. used bifacial DNA origami to assemble 3D anisotropic gold nanorod (AuNR) dimers for first time [143]. Through precisely tuning the location of AuNRs on origami, the distinct plasmonic CD response was observed in a spatial configuration dependent manner (Fig. 16d). Subsequently, they constructed anisotropic AuNR helices by changing the molar ratio of AuNR/origami [144]. After increasing the number of AuNRs in the assembly system from 2 to 9, the chiroptical activity enhanced (Fig. 16e). The anisotropy factor could reach ~0.02, which was comparable to the macroscopic AuNRs.

Various chiral structures can be obtained by arranging multiple nanoparticles in a spiral direction. In 2012, Ding et al. firstly constructed 3D chiral nanostructures by transforming 2D rectangular origami into tubular origami [145]. Two liner AuNP chains were anchored at specific position of 2D DNA origami. As 2D origami rolled into tube, the liner AuNP chains were arranged into 3D helix (Fig. 17a). In 2012, Liedl et al. produced chiral plasmonic nanostructures through arranging nine AuNPs (10 nm) on the surface of 24-helix bundle [146]. The resulting left- and right-handed helices of AuNPs showed characteristic bisignate signatures in visible region. After electroless deposition of same metal, the helices made from the enlarged 16 nm AuNPs displayed 400-fold increase of signal strength (Fig. 17b). When deposition silver onto AuNPs, the CD spectra shifted into blue region. That is because silver has a shorter

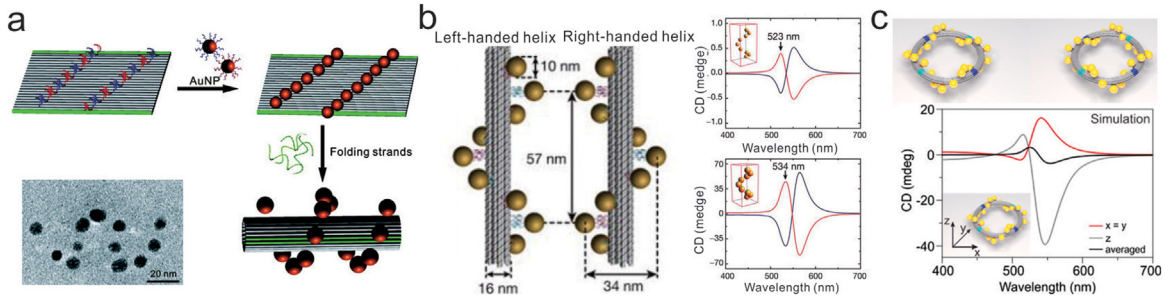

Fig. 17. 3D plasmonic chiral nanostructures. a) Rolling-up AuNPs-dressed DNA origami into 3D plasmonic chiral nanostructures. Reprinted with permission from ref. [145] Copyright © 2012, American Chemical Society. b) Left- and right-handed nanohelices formed by attaching AuNPs on 24-helix bundles. Reprinted with permission from ref. [146] Copyright © 2012, Springer Nature. c) Self-assembly of left- and right-handed plasmonic toroidal metamolecules. Reprinted with permission from ref. [148] Copyright © 2016, American Chemical Society.

plasmonic resonance wavelength than gold. Later on, they realized reversibly switching the CD response of left-handed nanohelices (L-NH) through attaching one end of the helix on the glass substrate [147]. The alignment of L-NHs was parallel to the glass when the glass was dry, and perpendicular in solution. Thus, the CD spectra was inverted to the switching light beam. Liu et al. constructed plasmonic toroidal metal nanostructures with four identical AuNP helices [148]. The metal nanostructures exhibited optical activity, and their enantiomers yielded opposite CD response. Moreover, the complete toroidal structure had stronger chiroptical response than their monomers and dimers building blocks (Fig. 17c).

Reconfigurable plasmonic systems possess dynamically controlled CD response. In 2017, Ding et al. found stimulus-responsive plasmonic chiral signals of AuNRs organized on DNA origami [149]. The geometry and chiral signals responded to multiple stimuli. Glutathione or restriction enzyme dissociated of the rhombus into two triangular origami, thus induced irreversible CD signal changes. While pH and light triggered reversible changes through the stretching and folding of metal nanostructures (Fig. 18a). In a work proposed by Liu et al., ssDNA could serve as fuel to drive the plasmonic nanostructures to certain state [150]. Through strand displacement reaction, the angle between two bundles as well as the bound AuNRs would be altered. Therefore, the plasmonic nanostructure was driven to either left- or right-handed conformation (Fig. 18b). Static origami could also rearrange AuNRs. Liu's group made AuNR stepwisely walk directionally, progressively and reversely on 2D or 3D DNA origami [151]. The movements of the walker triggered a series of conformational changes of the system and activated near-field interaction changes between the stator and walker. Then the subsequent spectral changes could be read out (Fig. 18c).

SERS

The research shows that rough surface of gold, silver and cooper can significantly enhance the Raman signal, which is called Surface Enhanced Raman Spectroscopy (SERS). SERS can be used to analyze molecules with concentrations at nanometer scale, and can be applied in environmental analysis, explosive detection, food quality analysis and so on [152]. However, the Raman signal was hard to be separated from background without amplification as the scattering cross was small. Through putting the Raman active molecules in plasma hot spot, the Raman signal can be greatly enhanced, with enhancement factor over 10^{10} [153]. Normally, as the size of gaps decrease, the Raman enhancement effect increases, especially for the gap less than 1 nm [154]. Based on DNA self-assembly, strong SERS signal can be achieved by the plasma nanostructures with narrow gap.

Lim et al. used ssDNA to tune the gap among metal nanoparticles. In 2009, they synthesized gold-silver core-shell nanodumbbells for SERS-based molecule detection [155]. At the beginning, AuNP heterodimers (20 and 30 nm) were synthesized by DNA hybridization, while a single Raman active Cy3 molecule was anchored between the two dimers precisely. Then Ag shells were formed on the surface of AuNP to control the size of gaps. With 5 nm Ag shell, no obvious gap was found under atomic force microscopy (AFM), and the enhancement factor was 2.7×10^{12} (Fig. 19a). Subsequently, to realize stable and reproducible SERS detection, they constructed gold nanobridged nanogap particles (Au-NNP) with DNA modified AuNPs [154]. The well-formed gap between gold core and shell was ~1 nm, which could load specified number of Raman dyes. SERS signals were sensitive to 10 fM probe concentrations and the enhancement factors was 1.0×10^8~5.0×10^9 (Fig. 19b). Further investigation revealed that DNA bases to Au core and DNA grafting density on Au surface played important roles in controlling the Au shell and gap size. Ploy T created a narrower gap than poly A and ploy C. Low DNA grafting density formed no interior gap. Then they used T_{10} sequence modified Au-NNP to realize high-resolution live cell Raman imaging by high-speed confocal Raman microscopy without any significant cell damage [156].

2D DNA origami can be used to assemble metal nanoparticles with narrow interspace. According to the first report by Finkelstein, AuNPs were placed on the corners of rectangular origami precisely, and then enlarged by metal deposition [157]. Thus, 'hot spots' were formed between the adjacent nanoparticles, and Raman signal of 4-aminobenzenethiol molecules deposited on the nanoparticles was enhanced at least 100-fold (Fig. 19c). Feldmann et al. constructed plasmonic nanoantenna composed of a three-layered origami and two AuNPs on both sides. With a distance of 6 nm between AuNPs, Raman signal of the intercalated SYBR Gold molecules was enhanced 2×10^6 in the center [158] (Fig. 19d). By a $40 \times 45\ nm^2$ DNA origami platform, Keyser et al. confined the gap between two 40 nm AuNP of 3.3 ± 1 nm [159]. Raman signal of Rhodamine 6 G was increased by 10^5~10^7 times compared with molecules out of the hot spot. Lohmüller et al. furtherly controlled the gap between two AuNPs of 1~2 nm through optothermal induced shrinking of DNA origami [160]. The Raman signal of Cy 3.5 molecules placed in hot spot was increased by ~10^2 times when reducing gap size from 2.5 to 1.4 nm.

Gold nanomaterials with sharp tips have much higher electric field enhancement and thus better SERS efficiency than spherical and rod AuNPs. Sen et al. assembled two Au nanostars on dimerized DNA origami [161]. With Texas Red dye anchored in the conjugation region, the SERS enhancement factors are 2×10^{10} and 8×10^9 corresponding to the interparticle gaps of 7 and 13 nm in comparation to monomeric Au nanostar (Fig. 19e). More recently, Ding et al. assembled two Au nanoprisms into Au Bowtie nanoantennas in a tip-to-tip model [162]. With a gap between the tips of ~5 nm, Raman signal of the single probe set at the gap was enhanced 2.6×10^9 (Fig. 19f). Besides, the bowtie gold nanostructures fab-

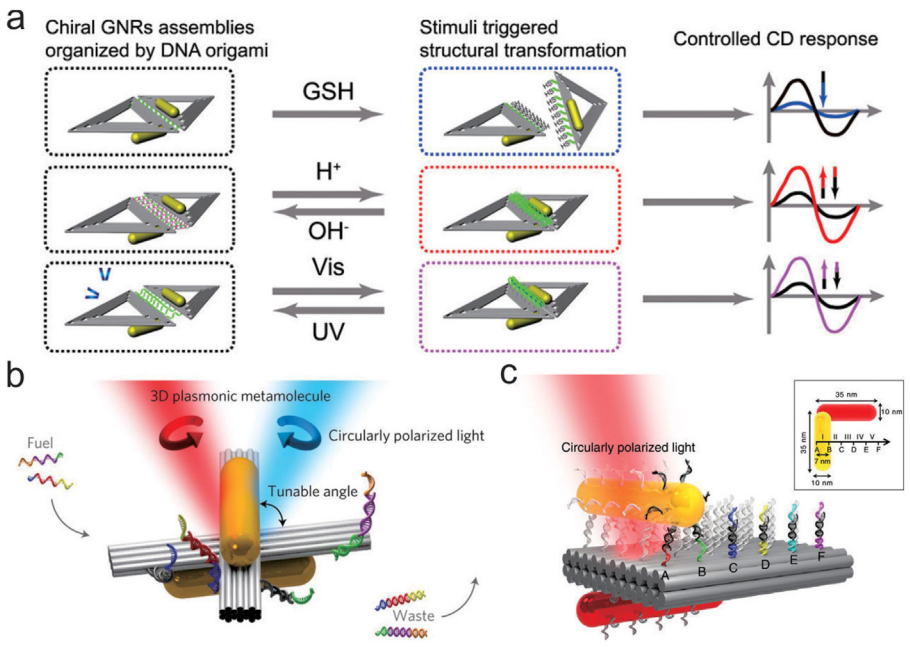

Fig. 18. Reconfigurable plasmonic systems. a) Stimulus-triggered plasmonic chiral signals changes of DNA origami-AuNRs. Reprinted with permission from ref. [149] Copyright © 2017, American Chemical Society. b) Reconfigurable 3D plasmonic metamolecules by DNA strands. Reprinted with permission from ref [150]. Copyright © 2014, Springer Nature. c) A plasmonic nanorod walking on DNA origami inducing spectral response changes. Reprinted with permission from ref [151]. Copyright © 2015, Springer Nature.

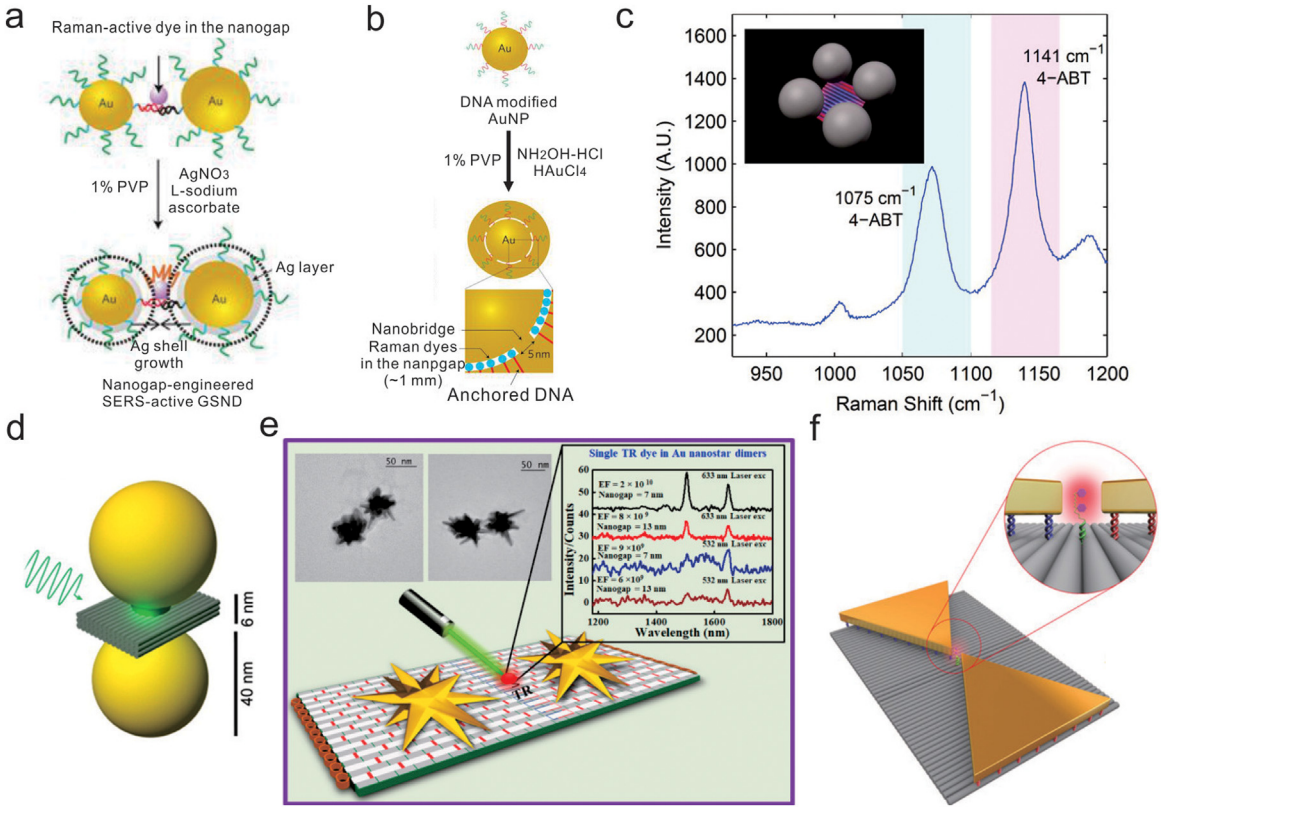

Fig. 19. SERS enhancement of metal systems. a) Nanogap-engineerable Raman active nanodumbbells based on gold-silver core-shell structures. Reprinted with permission from ref. [155] Copyright © 2009, Springer Nature. b) DNA-anchored nanobridged nanogap particles with 1-nm interior gap for SERS enhancement. Reprinted with permission from ref [154]. Copyright © 2011, Springer Nature. c) AuNP tetramers assembled on rectangular origami for SERS enhancement. Reprinted with permission from ref [157]. Copyright © 2014, American Chemical Society. d) Plasmonic DNA origami nanoantennas with a separation distance of 6 nm between two AuNPs. Reprinted with permission from ref [158]. Copyright © 2014, American Chemical Society. e) Au nanostar dimers on DNA origami for single-molecule SERS. Reprinted with permission from ref [161]. Copyright © 2017, American Chemical Society. f) Au bowtie nanoantennas for single molecule SERS. Reprinted with permission from ref [162]. Copyright © 2018, John Wiley and Sons.

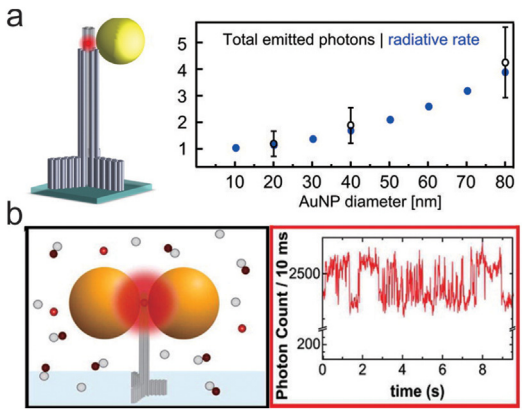

Fig. 20. Fluorescence enhancement. a) DNA origami-AuNP hybrids for controlled reduction of photobleaching via changing the sizes of AuNPs. Reprinted with permission from ref. [165] Copyright © 2014, American Chemical Society. b) DNA origami nanoantennas for fluorescence enhancement and single-molecule detection. Reprinted with permission from ref [168]. Copyright © 2015, American Chemical Society.

ricated by DNA-assisted lithography also formed hot spot between tips. The characteristic spectra of two SERS markers (rhodamine 6 G and 2,2-bipyridine) were detected with high resolution at the bowtie antennas area, while no Raman signal was detected from bare areas on the chip.

Fluorescence enhancement

Due to the Localized Surface Plasmon Resonance (LSPR) of metal nanomaterials, enhanced surface electric field may affect the local environment of surrounding molecules. Thus, the fabricated plasmonic structures can be employed to manipulate molecular fluorescence, which was depended on the material structure, size, geometry and position to the fluorescence. Regulation of the relative position of fluorescence and plasma nanomaterials through DNA nanotechnology was crucial to study the interaction between light and matter.

On one hand, non-radiative decay is accelerated by the interaction of fluorophore with local plasma electron, resulting in severe fluorescence quenching. This quenching has been used to make optical rulers for measuring subtle changes in biological systems [163]. Tinnefeld et al. studied distance-dependent fluorescence quenching between a fluorophore and a metal nanoparticle by immobilizing them on DNA origami [164]. When the distance was smaller than 15 nm, the fluorescence intensity was significantly quenched and the fluorescence lifetime was reduced. While this phenomenon disappeared for longer distance between the AuNP and fluorophore. Photobleaching refers to the decrease of the fluorescence intensity or interruption of the fluorescence emission in single molecule study. Reducing photobleaching is vital for fluorescence-based applications. The total number of emitted photons before photobleaching is proportional to the radiative decay rate of fluorophores. Tinnefeld's group used DNA origami pillar to control the distance between single AuNP and Cy5 dye of 8.5 nm [165]. Through changing the size of AuNPs, they found 20 nm AuNP had little effect to total photons, while 80 nm AuNP emitted photons four times more than those before photobleaching (Fig. 20a). Liddle et al. assembled AuNPs and CdSe/ZnS Quantum dots (QD) on 2D DNA origami [166]. Different location, number, size of AuNPs, interparticle distance and spectral overlap between AuNP-QD conjugates determined the fluorescence lifetime of QDs.

On the other hand, enhanced electric fields increase the intensity of photoluminescence when fluorophore is placed near the plasma nanoparticles. Fluorescence enhancement has great potential in biosensing and detection of molecules at low concentrations [167]. Optical nanoantennas could focus freely propagating light and improve the emission of the light source confined at hotspot. Tinnefeld et al. assembled 100 nm AuNP dimers on DNA origami pillar [168]. A single ATTO647 N was set at the center of interparticle gap. After reducing interparticle distance and optimizing quantum-yield, over 5000-fold fluorescence enhancement was achieved, and single-molecule detection limit reached 25 μM (Fig. 20b). Apart from fluorescence dyes, they also placed natural light-harvesting systems (peridinin-chlorophyll *a*-protein, PCP) into the hotspot based on AuNP or AgNP dimers as above mentioned [169]. When PCP was excited at 640 nm, they found the plasmon-induced fluorescence enhancement was 500-fold for AuNP dimers, which was the highest value reported for light-harvesting systems.

Enzyme cascade reaction

Enzyme cascade reaction refers to the product of the first enzyme acting as the substrate of the second enzyme [170]. The catalytic efficiency of multienzyme complexes mainly depends on the spatial organization. Self-assembled DNA nanostructures precisely control the position and orientation of the enzymes at nanoscale. The relative distance and compartmentalization of multienzymes, as well as substrate diffusion would affect the enzymatic reaction efficiency.

Willner et al. assembled hexagon-like DNA strips as scaffolds for hybridizing multienzyme complexes [171]. The widths of two-hexagon and four-hexagon DNA strips were ~13 nm and ~33 nm, respectively. The first anchored system was glucose oxidase (GOx) and horseradish peroxidase (HRP). GOx catalyzes the oxidation of glucose to gluconic acid. At the same time, H_2O_2 was formed, which was the substrate for HRP to oxidize 2'2'-azino-bis[3-ethylbenzthiazoline-6-sulphonic-acid] ($ABTS^{2-}$) to the colored product ABTS-. According to the result, the oxidation efficiency of $ABTS^{2-}$ on two-hexagon structures was ~1.2-fold higher than that on the four-hexagon structures. The second system was glucose dehydrogenase (GDH)-NAD^+. GDH oxidizes glucose to gluconic acid and reduces NAD^+ to NADH simultaneously. The resulting NADH reduces methylene blue (MB^+) to colorless MBH. Through varying the length of tethers linking NAD^+ to the scaffold, they found it led to the less efficient communication between GDH and NAD^+ by reducing the tethers (Fig. 21a). Yan et al. assembled GOx/HRP enzymes on DNA rectangular origami with different interspaces. The reaction activity was enhanced as the distance between enzymes was reduced [172]. More importantly, they found the effective transfer of intermediate H_2O_2 was essential to the reaction activity. Thus, a noncatalytic protein bridge was set between the enzymes to reduce the diffusion of H_2O_2. With a β-galactosidase (β-gal) bridge anchored between the enzyme pairs, the activity was ~42 ± 4% higher compared with the enzymes without the bridge (Fig. 21b). Apart from passive diffusion of the intermediates from one enzyme to another, the same group used a ssDNA 'swinging arm' to carry the substrate and transfer it to the next enzyme, which improves the enzymatic activity [173]. In a typical G6pDH/MDH enzyme cascade reaction, NAD^+ modified ssDNA was positioned right in the middle between the two enzymes to facilitate the transfer of NAD^+/NADH (Fig. 21c).

Tubular DNA origami has been used as efficient enzyme cascade nanoreactors similarly. In 2013, Fu et al. wrapped rectangular origami into 1D nanotubes, with GOx/HRP system being assembled inside the tubes [174]. They found the enzymes anchored within the nanotubes were more reactive than semiconfined on planar origami. The activity enhancement was not only the stabi-

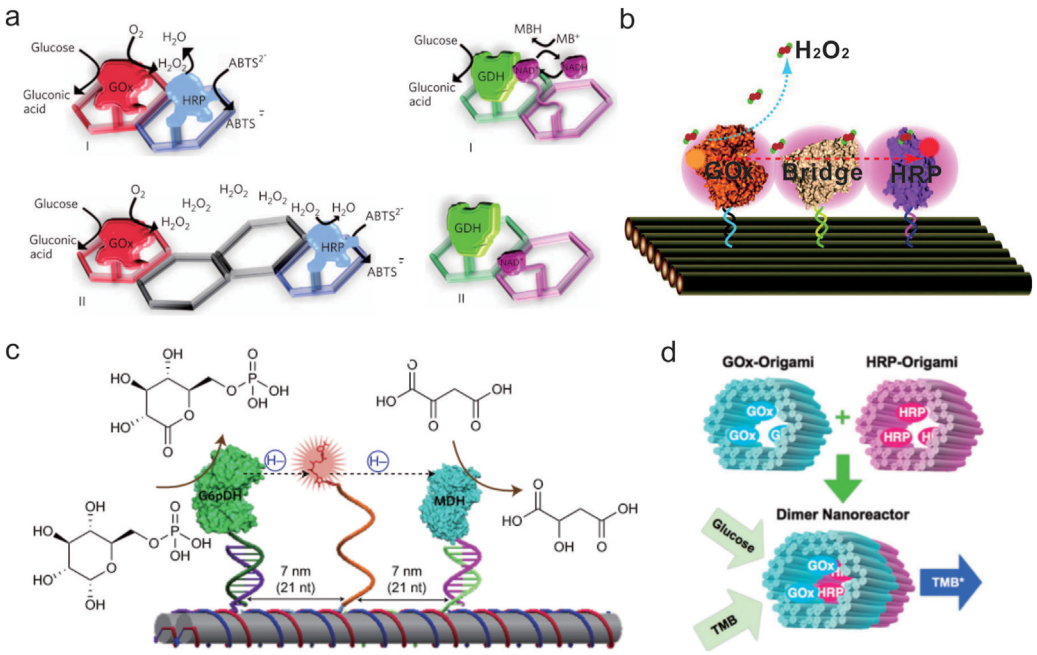

Fig. 21. Enzyme cascade reaction with DNA nanostructures-enzymes hybrids. a) Enzyme and cofactor-enzyme cascades on hexagon-like DNA strips. Reprinted with permission from ref. [171] Copyright © 2009, Springer Nature. b) Limited diffusion of H_2O_2 through a protein bridge. Reprinted with permission from ref. [172] Copyright © 2012, American Chemical Society. c) NAD^+-modified ssDNA swinging arm restriction the diffusion of NAD^+/ NADH between two enzymes. Reprinted with permission from ref. [173] Copyright © 2014, Springer Nature. d) Tubular DNA origami-based enzymatic cascade nanoreactor. Reprinted with permission from ref [175]. Copyright © 2015, Royal Society of Chemistry.

lizing effect of DNA nanostructure, the caging effect of the confined nanospace also played a crucial role. Linko et al. developed a dynamic control system, in which GOx and HRP were anchored in two tubular DNA origami units separately and linked together to form a complete bioreactor [175] (Fig. 21d).

Drug delivery

Thanks to the high biostability, biocompatibility and cell uptake efficiency, DNA nanostructures have been used as carriers for a variety of therapeutic molecules, including inorganic nanoparticles and protein.

Photothermal therapy (PTT) employs light absorbing agents to achieve photothermal damage of tumors. When PTT agents absorb light, electrons transited from ground state to excited state. The electronic excitation energy relaxes through nonradiative channels, which lead to the overheating of local environment around PTT agents. The heat causes irreversible cell damage or tissue destruction [176]. In recent years, AuNPs and AuNRs have become very useful PTT agents in plasmonic photothermal therapy [177,178]. It is due to their strong adsorption in visible and NIR region. However, the biggest disadvantage of this therapy is its low selectivity to target tissue. DNA origami could be excellent carrier because of its passive targeting effects to tumors and high cell uptake efficiency. Thus, the origami-AuNR complex (DO-AuNR) integrated optical photothermal effects of AuNR with passive tumor targeting and long-lasting accumulation of origami. Ding et al. constructed a dual-functional theranostic platform by assembling AuNRs on the surface of DNA origami [179]. This platform possessed two-photon cell imaging and photothermal effect. According to their results, DO-AuNR showed better internalization than bare AuNR in breast cancer cells through two-photon luminescence imaging. Moreover, enhanced photothermal therapy efficacy was achieved by DO-AuNR under NIR laser irradiation during in vitro and in vivo experiments (Fig. 22a). Because of the LSPR, AuNRs also have strong optoacoustic signal generation and photo stability. Subsequently, they demonstrated that optoacoustic imaging (OAI) technique provided by DO-AuNR could be utilized for tumor imaging, with high spatial resolution and enhanced depth of imaging penetration [180].

As the vulnerability to degradation and poor membrane permeability of proteins, a non-invasive delivery route is desirable. DNA nanostructures have been developed to deliver antigen, antibody and transcription factor protein into cells [181–183]. In a research from Zhao et al., thrombin was assembled inside the DNA robot and transported to tumors with high targeting efficiency [184]. DNA aptamers on the nanorobot could bind with nucleolin, proteins specifically expressed on the surface of tumor cells. This nucleolin-targeting aptamer served as a trigger for mechanical opening of the DNA nanorobot. Then the thrombin inside the robot was exposed and resulted in tumor necrosis and inhibition of tumor growth eventually (Fig. 22b).

Gene therapy uses foreign nucleic strands as medicine to repair defective genes, however their safe and efficient delivery is the major challenge. Qu et al. believed that DNA-templated silver metallization would induce curvature and condensation of DNA, as well as neutralization of the negative charges of DNA strands [185]. This DNA-templated silver metallization was favorable for cellular internalization. Then the thiol groups of glutathione (GSH) molecules was used to release DNA through ligand exchange process, in which the formation of robust Ag-S bonds would remove silver deposition from DNA. By this way, they transfected EGFP plasmid (pEGFP) into cells, and the result showed that the transfection efficiency of pEGFP-silver was comparable to the commercial transfection reagent Lipofectamine 2000. This work implied that DNA-silver could be low cytotoxicity and highly efficient delivery agents (Fig. 22c)

Bioimaging

QDs serve as bright luminophores benefiting from their wide quantum size-effect tunability, and possess composition- and size-

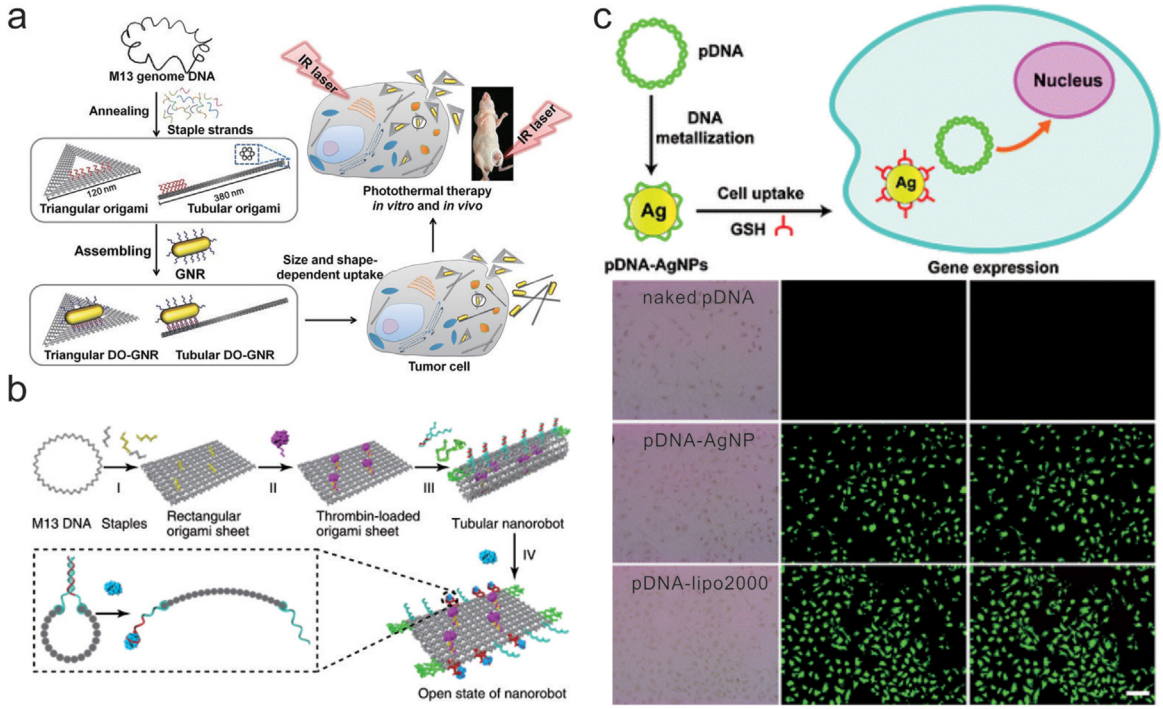

Fig. 22. DNA origami as drug carriers. a) DNA origami-AuNR complex for two photon cell imaging and photothermal therapy. Reprinted with permission from ref. [179] Copyright © 2015, John Wiley and Sons. b) Thrombin-functionalized DNA nanorobot for cancer therapeutic. Reprinted with permission from ref [184]. Copyright © 2018, Springer Nature. c) Metallized plasmid DNA for efficient gene delivery. Reprinted with permission from ref [185]. Copyright © 2013, Royal Society of Chemistry.

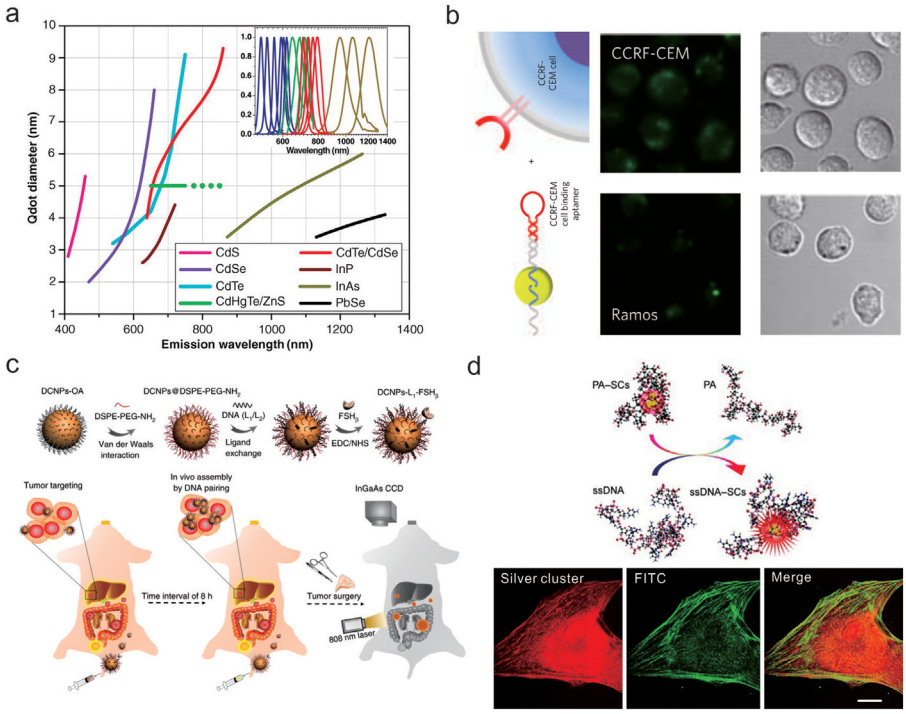

Fig. 23. DNA-based nanoparticles and nanoclusters for bioimaging. a) Maximum emission of QDs with different sizes and compositions. Reprinted with permission from ref. [186] Copyright © 2005, The American Association for the Advancement of Science. b) Aptamer-functionalized QDs for cell-targeting imaging. Reprinted with permission from ref. [63] Copyright © 2008, Springer Nature. c) In vivo assembly of NIR -II nanoprobes for improved image-guided surgery. Reprinted with permission from ref [191]. Copyright © 2018, Springer Nature. d) Shuttle-based silver nanoclusters for actin imaging. Reprinted with permission from ref [193]. Copyright © 2009, John Wiley and Sons.

dependent absorption and emission feature [186] (Fig. 23a). Thanks to the brightness and photostability, QDs can be widely applied in optical detection, energy harvesting and biological imaging. With the optimization of imaging equipment [187,188], functionalization of DNA would be beneficial to QDs for probing special cell components and tumors *in vivo*.

DNA functionalized QDs can be used as bio-probes for applications in diagnostics and bio-imaging. Especially DNA aptamer-functionalized QDs possess specific binding affinity to cognate cells. Kelley et al. modified QDs with specific aptamers to distinguish CCRF-CEM cells (T cell line, human acute lymphoblastic leukaemia) from Ramos cells (B cell line, human Burkitt's

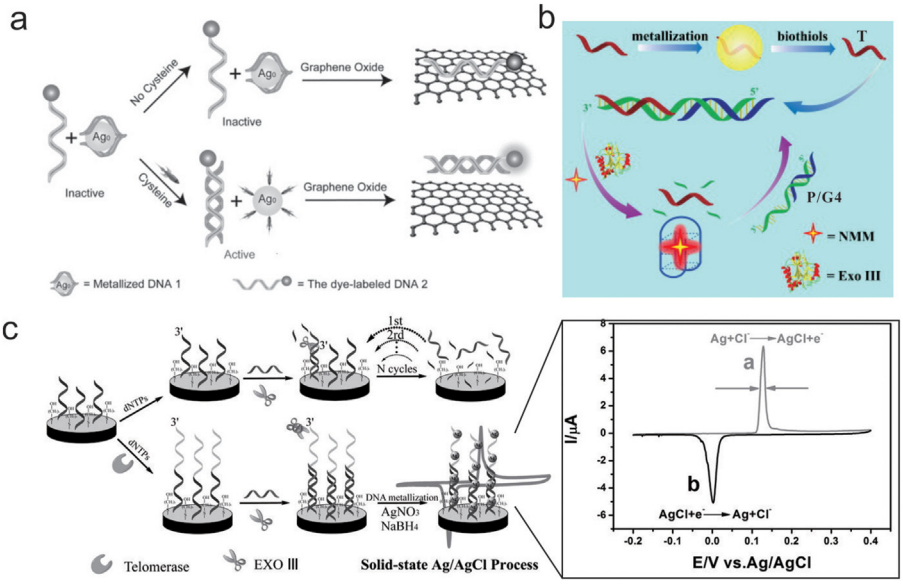

Fig. 24. Biodetection through DNA metallization. a) Sensitive turn-on fluorescence detection of cysteine with the combination of graphene oxide and DNA metallization. Reprinted with permission from ref. [202] Copyright © 2011, John Wiley and Sons. b) Amplified detection of biothiols with the help of Exonuclease III and DNA metallization. Reprinted with permission from ref. [203] Copyright © 2014, Elsevier. c) Ultrasensitive detection of telomerase activity based on DNA metallization and characteristic solid-state electrochemical techniques. Reprinted with permission from ref. [205] Copyright © 2014, John Wiley and Sons.

lymphoma) [63]. Optical imaging of aptamer functionalized QDs showed quantitative differences between these two cells (Fig. 23b). In Fan's work, the assemblies of monovalent QDs and DNA-primary antibody incubated with cells with or without secondary antibody, respectively [64]. Fluorescent images exhibited that QDs produced clear imaging of microtubules in samples with secondary antibody. Some second-window near-infrared fluorescence probes (NIR-II, 900–1700 nm) have good application prospect for in vivo imaging, due to their high tissue penetration depth and low tissue autofluorescence [189,190]. Zhang et al. modified NIR-II downconversion nanoparticles (DCNPs) with ssDNA (L1 or complementary L2 separately) through ligand exchange and tumor targeting peptide (FSH_β) by covalent conjugation [191]. After two-staged injection of DCNPs-L1- FSH_β and DCNPs-L2- FSH_β with time interval of 8 h, the two nanoprobes hybridized in vivo. The larger assembled superstructures contributed to higher tumor targeting efficiency and longer tumor retention time, which would improve image-guided surgery (Fig. 23c).

Apart from QDs, silver-nanocluster from ssDNA metallization also have excellent brightness and photostability [192]. As the reduction agents BH_4^- ion may destroy the function of proteins in cells, Dickson et al. developed a shuttle-based method for silver-cluster imaging [193]. The clusters were firstly synthesized on polyacrylic acid (PA), then transferred to ssDNA-protein conjugates with simple mixing. When conjugating with anti-actin antibody, the ssDNA-based silver-clusters located on the actin of cells and colocalized well with FITC-antibody (Fig. 23d).

Biodetection

Highly sensitive and selective detection of biomarkers is vital in the early diagnose of diseases [194–200]. For example, abnormal level of biothiols (cysteine, homocysteine and glutathione) indicated the occurrence of many diseases, such as cancer and heart disease [201]. On one hand, biothiols could retrieve DNA from its blocked state in silver depositions. Thus, DNA-templated Ag metallization has applied in biodetection for biothiols. In 2011, Qu et al. developed a detection system consisting of graphene oxide (GO), silver metallized DNA1 and complementary fluorescent DNA2. In the absence of cysteine, as the silver deposition disrupted the hybridization of DNA1 and DNA2, GO would quench the fluorescence of DNA2 through π-stacking. While in the presence of cysteine, it replaced Ag clusters from DNA1 through forming strong Ag-S bonds, thus the released DNA1 could conjugate with fluorescent DNA2 [202] (Fig. 24a). As GO possessed different affinity for ssDNA and dsDNA, the fluorescence of DNA2 would not be quenched. Such a turn-on method achieved 2 nM detection limit for cysteine. Subsequently, they designed another detection system by combining DNA metallization and Exonuclease III (Exo III), which selectively digest 3'-end of dsDNA [203]. When biothiols existed, target DNA (T) would be released form silver clusters. This DNA would hybridize with its complementary parts in probe P/G4. The hybridization led to the expose of blunt 3'-end, which was digested by Exo III. Thus, the quadruplex oligomers (G4) would be released. N-methyl mesoporphyrin IX (NMM) interacted with G4 and produced fluorescence enhancement for signal readout eventually (Fig. 24b). This amplified detection of biothiols could reach picomolar concentration.

On the other hand, DNA-templated metallization could increase the amount of metal traces and thus amplify the electrochemical response [204]. Qu et al. presented ultrasensitive electrochemical method for telomerase activity detection in circulating tumor cells [205]. In their design, the telomerase primer sequences were initially anchored on Au electrodes through Au-S bonds. Then the electrodes were placed in solution containing telomerase and dNTPs for elongation of the primers. Ag^+ in solution was absorbed on elongated primers and reduced to silver clusters along the DNA sequences. The subsequent solid-state voltammetric method showed two well separated sharp current peaks, which attributed to the oxidation of Ag to AgCl and reduction of AgCl to Ag. In order to improve the signal-to-noise ratio, complementary strands were added to hybridize with primers and generate blunt 3'-end. Exo III digested the unextended primers and released complementary strands for further removal. Thus, the background signals could be suppressed (Fig. 24c). Zhang et al. detected sequence-specific DNA by hybridizing it with peptide nucleic acid immobilized on gold electrode [206]. With hemin as efficient biomimetic catalyst to accelerate the reduction of Ag^+, silver clusters would deposit on the electrode. Measured by square wave voltammetry in KCl solution, the detection limit reached 62.41 aM.

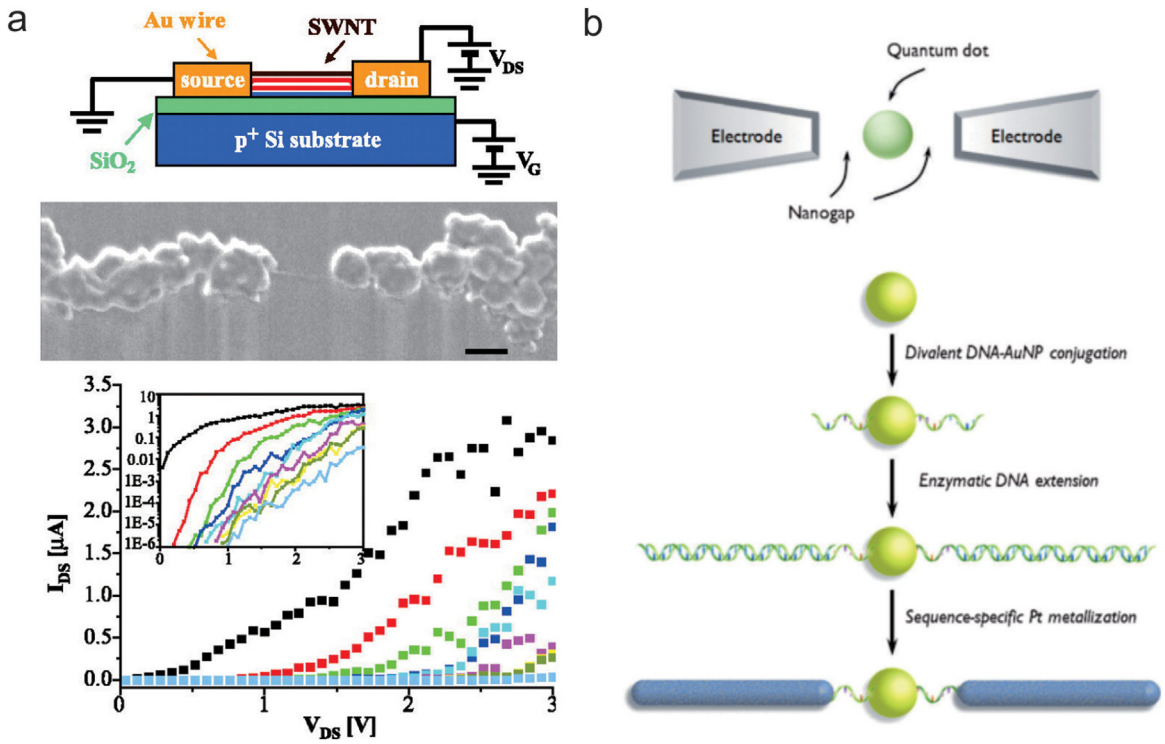

Fig. 25. Conducting devices fabricated by DNA metallization. a) Carbon nanotube field-effect transistor based on DNA templated Au metallization. Reprinted with permission from ref. [207] Copyright © 2003, The American Association for the Advancement of Science. b) Fabrication of double tunnel junction single-electron device by Pt metallization of divalent DNA-AuNP conjugates. Reprinted with permission from ref [208]. Copyright © 2012, John Wiley and Sons.

Conducting devices

After Braun et al. proposed DNA-templated metallization endowed DNA with electrical conductivity, metal nanostructures possessed the potential as conductive nanodevices. They reported a carbon nanotube field-effect transistor based on DNA metallization, which would improve the precise location of sing-wall carbon nanotubes (SWNT) and assembly the SWNT into large-scale nanodevices [207]. Briefly, SWNT was located in the dsDNA scaffold by interacting with RecA proteins bound on specified sites of DNA scaffold. As RecA proteins resisted the Ag^+ reduction, electrical measurement circuit was constructed by individual SWNT, which was connected by two DNA-templated Au nanowires (Fig. 25a). A single-electron device allows one charge to be transported through. It composes of tunneling junctions that made of metal islands separated by insulating barriers. However, it's challenging to position a metal island between two electrodes with controlled distance. Ijiro et al. fabricated single-electron devices via metallization of divalent DNA-nanoparticle conjugates [208]. In their design, two polyG and polyC dsDNA sequences assembled on 5 nm AuNP were extended, leaving an ssDNA portion and extended polyG and polyC dsDNA portion. Subsequent Pt deposition on purine bases of DNA sequences produced double tunnel junction, in which the AuNP was separated from the Pt structures by two ssDNA strands (Fig. 25b). Fitzmaurice et al. assembled a protein-functionalized electrode with 10 nm gap [209]. Modified AuNPs were adsorbed on the SH-DNA-biotin template, and AuNPs located at the biotin sites was replaced by streptavidin. Thus, after metallization, there was a nanogap in the streptavidin-functionalized electrodes. Other biotin modified AuNPs could be anchored in the nanogap through interaction with streptavidin.

DNA metallization produced metal clusters could be cathode or anodes materials for fuel cells. Bhat et al. realized DNA-based Pt metallization on graphite nanofibers, which could be used as oxygen reduction catalyst for polymer electrolyte fuel cells (PEFC) [210]. The excellent dispersion of Pt nanoparticles resulted in enhanced cathode catalytic performance in H_2-O_2 PEFC, with a peak power density of 675 mW cm^{-2}. And Pd growth on carbon nanotubes also served as cathode materials [211]. Choi et al. constructed Li-ion battery anodes with nickel oxide nanostructures based on DNA metallization [212]. The metal nanostructure delivered reversible capacity of 850 mA h g^{-1}, which was even higher than current graphite anodes. Also, ssDNA-templated Pt [213] and Pd [214] metallization on graphene could fabricate anodes materials for fuel cells.

Conclusions and future perspectives

Since its inception, DNA nanostructures have become excellent templates for nanofabrication. In this review, we make a thorough overview of recent advances in large-scale assembled DNA nanostructures, and the principle for DNA-based nanofabrication as well as their subsequent applications. Undoubtedly, the 1D, 2D and 3D expanded nanostructures provide numerous external and internal reaction sites. A spatial resolution of 5-nm confers accuracy for programmable functionalization. The relatively high biocompatibility, biostability and cell uptake efficiency of DNA nanostructures allow them work efficiently in biological systems. Based on these advantages, DNA nanostructures have great potential in the development of nanodevices in geometrical precise control related applications, such as conducting nanodevices, bioimaging, biodetection and drug delivery.

Despite these exciting achievements, the DNA-templated nanofabrication is still in its infancy and has a long way to go before they can be used in real applications. We briefly summarize the challenges need to be addressed at present:

1) It should be admitted that the large-scale assembled DNA nanostructures were largely restricted in the range of 100 nm~10 μm,

which limits their practical applications. Thus, alternative strategies need to be developed for size expansion.

2) Current technologies mainly utilize λ-DNA as templates for metallization. There are many limitations to realize DNA origami metallization both in solution and on surface, for instance, chemical stability. Thus, developing moderate conditions for DNA metallization would be helpful. What's more, reports on site-specific metallization that takes advantage of the addressability of DNA nanostructures are very rare. Modification functional groups to bind metal ions on DNA nanostructures may facilitate site-specific metallization.
3) DNA is relatively expensive compared to other inorganic materials. Especially for functional nucleic acids, such as thiols, amino, biotin groups and fluorescent dyes. Therefore, economic DNA mass production as well as development of simple yet robust methods for DNA modification are extremely necessary. In vivo production of DNA strands and even DNA nanostructures may solve this issue [215].
4) Physical conditions that contain insufficient cationic ions and abundant DNA nucleases would extremely affect the stability of DNA nanostructures. Although very recent report showed that certain DNA nanostructures can withstand low ion concentration environment for a while [216]. In addition, proteins coating on DNA nanostructures could form "protein corona" in physical environment, to protect structures dissociation and nuclease digestion [217].
5) The ultimate fate of DNA nanostructures in cells need to be further explored, as many studies showed DNA nanostructures transported to lysosome for digestion [218]. Lysosomal escape in an efficient and safe way would be necessary for releasing cargo into the cytosol and nucleus. Potential strategies include using targeting molecules to initiate a non-lysosomal uptake pathway or conjugating functional molecules on DNA origami for lysosomal escape.

While challenges remain, we have seen the evolution of DNA based nanofabrication from simple systems toward advanced applications in the past years. By combining with other materials, it is expected to bring a dramatic change to human manufacturing.

Acknowledgements

The authors thank the National Key R&D Program of China (Grant No. 2016YFA0201200), the National Natural Science Foundation of China (Grant No.21603262) and Lu Jiaxi International Team for financial support.

References

[1] D. Mijatovic, C.K.E. Jan, Vd.B. Albert, Lab Chip 5 (2005) 492–500.
[2] J.Y. Cheng, C.A. Ross, H.I. Smith, E.L. Thomas, Adv. Mater. 18 (2006) 2505–2521.
[3] S.Y. Wu, C.Y. Lin, M.C. Chiang, J.J. Liaw, J.Y. Cheng, S.H. Yang, et al., IEEE International Electron Devices Meeting, 2016, pp. 43–46.
[4] M. Shimomura, T. Sawadaishi, Curr. Opin. Colloid Interface Sci. 6 (2001) 11–16.
[5] J. Cai, P. Ruffieux, R. Jaafar, M. Bieri, T. Braun, S. Blankenburg, et al., Nature 466 (2010) 470–473.
[6] R. Liu, D. Wu, X. Feng, K. Muellen, J. Am. Chem. Soc. 133 (2011) 15221–15223.
[7] N.C. Seeman, Nature 421 (2003) 427–431.
[8] E. Stulz, Chem. Eur. J. 18 (2012) 4456–4469.
[9] C.H. Fan, H. Pei, Chin. J. Chem. 34 (2016) 251.
[10] N.C. Seeman, H.F. Sleiman, Nat. Rev. Chem. 3 (2017) 17068.
[11] P.B. Dervan, Bioorgan. Med. Chem. 9 (2001) 2215–2235.
[12] R.D. Blake, S.G. Delcourt, Nucleic Acids Res. 26 (1998) 3323–3332.
[13] P. Guo, Nat. Nanotechnol. 5 (2011) 833–842.
[14] K.A. Afonin, B. Eckart, A.J. Yaghoubian, V. Neil, J. Erica, B.A. Shapiro, et al., Nat. Nanotechnol. 5 (2010) 676–682.
[15] P.F. Wang, S.H. Ko, C. Tian, C.H. Hao, C.D. Mao, Chem. Commun. 49 (2013) 5462–5464.
[16] N.B. Leontis, S. Jesse, W. Eric, Nucleic Acids Res. 30 (2002) 3497–3531.
[17] W.W. Grabow, P. Zakrevsky, K.A. Afonin, A. Chworos, B.A. Shapiro, L. Jaeger, Nano Lett. 11 (2011) 878–887.
[18] C. Arkadiusz, S. Isil, A.Y. Koyfman, W. Patrick, O. Emin, H.G. Hansma, et al., Science 306 (2004) 2068–2072.
[19] H. Ohno, S. Akamine, H. Saito, Curr. Opin. Biotechnol. 58 (2019) 53–61.
[20] Y.G. Ke, L.L. Ong, W.M. Shih, P. Yin, Science 338 (2012) 1177–1183.
[21] N.C. Seeman, Acc. Chem. Res. 30 (1997) 357–363.
[22] T.J. Fu, N.C. Seeman, Biochemistry 32 (1993) 3211–3220, The DNA double-crossover molecules laid the foundation for many DNA nanostructures to become realistic.
[23] P.W. Rothemund, Nature 440 (2006) 297–302, The first experimental demonstration of spatially addressable 2D DNA origami.
[24] L.L. Ong, N. Hanikel, O.K. Yaghi, C. Grun, M.T. Strauss, P. Bron, et al., Nature 552 (2017) 72–77.
[25] Y. Yang, D. Han, J. Nangreave, Y. Liu, H. Yan, ACS Nano 6 (2012) 8209–8215.
[26] D. Han, X. Qi, C. Myhrvold, B. Wang, M. Dai, S. Jiang, et al., Science 358 (2017), eaao2648.
[27] A.N. Marchi, I. Saaem, B.N. Vogen, S. Brown, T.H. LaBean, Nano Lett. 14 (2014) 5740–5747.
[28] K.F. Wagenbauer, C. Sigl, H. Dietz, Nature 552 (2017) 78–83.
[29] B. Wei, M. Dai, P. Yin, Nature 485 (2012) 623–626.
[30] G. Tikhomirov, P. Petersen, L.L. Qian, Nature 552 (2017) 67–71.
[31] Y. Suzuki, M. Endo, H. Sugiyama, Nat. Commun. 6 (2015) 8052.
[32] C. Tian, C. Zhang, X. Li, C. Hao, S. Ye, C. Mao, Langmuir 30 (2014) 5859–5862.
[33] S. Woo, P.W.K. Rothemund, Nat. Chem. 3 (2011) 620–627.
[34] A.A. Rafat, T. Pirzer, M.B. Scheible, A. Kostina, F.C. Simmel, Angew. Chem. Int. Ed. 53 (2014) 7665–7668.
[35] P. Wang, S. Gaitanaros, S. Lee, M. Bathe, W.M. Shih, Y. Ke, J. Am. Chem. Soc. 138 (2016) 7733–7740.
[36] Y. He, Y. Tian, A.E. Ribbe, C.D. Mao, J. Am. Chem. Soc. 128 (2006) 15978–15979.
[37] J. Zheng, J.J. Birktoft, Y. Chen, T. Wang, R. Sha, P.E. Constantinou, et al., Nature 461 (2009) 74–77, The first successful experiment to create 3D DNA crystals through sticky-end routes.
[38] Y. He, Y. Chen, H.P. Liu, A.E. Ribbe, C.D. Mao, J. Am. Chem. Soc. 127 (2005) 12202–12203.
[39] G. Tikhomirov, P. Petersen, L.L. Qian, Nat. Nanotechnol. 12 (2016) 251–259.
[40] F. Hong, S. Jiang, X. Lan, R.P. Narayanan, P. Sulc, F. Zhang, et al., J. Am. Chem. Soc. 140 (2018) 14670–14676.
[41] F. Zhang, C.R. Simmons, J. Gates, Y. Liu, H. Yan, Angew. Chem. Int. Ed. 57 (2018) 12504–12507.
[42] T. Zhang, C. Hartl, K. Frank, A. Heuer-Jungemann, S. Fischer, P.C. Nickels, et al., Adv. Mater. 30 (2018), e1800273.
[43] P. Yin, R.F. Hariadi, S. Sahu, H.M.T. Choi, S.H. Park, T.H. LaBean, et al., Science 321 (2008) 824–826.
[44] N.R. Kallenbech, R.I. Ma, N.C. Seeman, Nature 305 (1983) 829–831, The first experimental demonstration of an immobile DNA junction.
[45] R.I. Ma, N.R. Kallenbach, R.D. Sheardy, M.L. Petrillo, N.C. Seeman, Nucleic Acids Res. 14 (1986) 9745–9753.
[46] Y.L. Wang, J.E. Mueller, B. Kemper, N.C. Seeman, Biochemistry 30 (1991) 5667–5674.
[47] X. Wang, N.C. Seeman, J. Am. Chem. Soc. 129 (2007) 8169–8176.
[48] M. Lu, Q. Guo, N.C. Seeman, N.R. Kallenbach, J. Mol. Biol. 221 (1991) 1419–1432.
[49] H. Yan, S.H. Park, G. Finkelstein, J.H. Reif, T.H. LaBean, Science 301 (2003) 1882–1884.
[50] D.G. Liu, M.S. Wang, Z.X. Deng, R. Walulu, C.D. Mao, J. Am. Chem. Soc. 126 (2004) 2324–2325.
[51] G. Tikhomirov, P. Petersen, L.L. Qian, J. Am. Chem. Soc. 140 (2018) 17361–17364.
[52] R. Sha, J.J. Birktoft, N. Nguyen, A.R. Chandrasekaran, J. Zheng, X. Zhao, et al., Nano Lett. 13 (2013) 793–797.
[53] S. Woo, P.W. Rothemund, Nat. Commun. 5 (2014) 4889.
[54] J. Li, S. Song, X. Liu, L. Wang, D. Pan, Q. Huang, et al., Adv. Mater. 20 (2008) 497–500.
[55] M.C. Daniel, D. Astruc, Chem. Rev. 104 (2004) 293–346.
[56] B.W. Liu, J.W. Liu, Anal. Methods 9 (2017) 2633–2643.
[57] J.J. Storhoff, R. Elghanian, R.C. Mucic, C.A. Mirkin, R.L. Letsinger, J. Am. Chem. Soc. 120 (1998) 1959–1964.
[58] J.I. Cutler, E. Auyeung, C.A. Mirkin, J. Am. Chem. Soc. 134 (2012) 1376–1391.
[59] X. Zhang, M.R. Servos, J.W. Liu, J. Am. Chem. Soc. 134 (2012) 7266–7269.
[60] B.W. Liu, J.W. Liu, J. Am. Chem. Soc. 139 (2017) 9471–9474.
[61] C. Zhang, R.J. Macfarlane, K.L. Young, C.H.J. Choi, L.L. Hao, E. Auyeung, et al., Nat. Mater. 12 (2013) 741–746, A general approach to create ssDNA shell on nanoparticles of various composition.
[62] H. Pei, F. Li, Y. Wan, M. Wei, H. Liu, Y. Su, et al., J. Am. Chem. Soc. 134 (2012) 11876–11879.
[63] N. Ma, E.H. Sargent, S.O. Kelley, Nat. Nanotechnol. 4 (2008) 121–125.
[64] J.L. Shen, Q. Tang, L. Li, J. Li, X.L. Zuo, X.M. Qu, et al., Angew. Chem. Int. Ed. 57 (2017) 16077–16081.
[65] K.H. Siu, R.P. Chen, Q. Sun, L. Chen, S.L. Tsai, W. Chen, Curr. Opin. Biotechnol. 36 (2015) 98–106.
[66] R. Meyer, S. Giselbrecht, B.E. Rapp, M. Hirtz, C.M. Niemeyer, Curr. Opin. Chem. Biol. 18 (2014) 8–15.

[67] R. Jungmann, M.S. Avendano, J.B. Woehrstein, M. Dai, W.M. Shih, P. Yin, Nat. Methods 11 (2014) 313–318.
[68] J.B. Trads, T. Tørring, K.V. Gothelf, Acc. Chem. Res. 50 (2017) 1367–1374.
[69] J. Fu, Y.R. Yang, S. Dhakal, Z. Zhao, M. Liu, T. Zhang, et al., Nat. Protoc. 11 (2016) 2243–2273.
[70] D.M. Bauer, I. Ahmed, A. Vigovskaya, L. Fruk, Bioconjugate Chem. 24 (2013) 1094–1101.
[71] E. Braun, Y. Eichen, U. Sivan, G.B. Yoseph, Nature 391 (1998) 775–778, The first experimental demonstration of DNA metallization.
[72] J. Richter, M. Mertig, W. Pompe, I. Mönch, H.K. Schackert, Appl. Phys. Lett. 78 (2001) 536–538.
[73] R. Schreiber, S. Kempter, S. Holler, V. Schuller, D. Schiffels, S.S. Simmel, et al., Small 7 (2011) 1795–1799.
[74] A. Stern, G. Eidelshtein, R. Zhuravel, G.I. Livshits, D. Rotem, A. Kotlyar, et al.,Adv. Mater. 30 (2018), e1800433.
[75] W.E. Ford, O. Harnack, A. Yasuda, J.M. Wessels, Adv. Mater. 13 (2001) 1793–1797.
[76] Y. Geng, J. Liu, E. Pound, S. Gyawali, J.N. Harb, A.T. Woolley, J. Mater. Chem. 21 (2011) 12126–12131.
[77] Q. Gu, C. Cheng, D.T. Haynie, Nanotechnology 16 (2005) 1358–1363.
[78] A.A. Zinchenko, D. Baigl, N. Chen, K. Endo, V.G. Sergeyev, O. Pyshkina, et al., Biomacromolecules 9 (2008) 1981–1987.
[79] H.D. Mohamed, S.M. Watson, B.R. Horrocks, A. Houlton, Nanoscale 4 (2012) 5936–5945.
[80] M. Mertig, L.C. Ciacchi, R. Seidel, W. Pompe, Nano Lett. 2 (2002) 841–844.
[81] Q. Gu, C. Cheng, S. Suryanarayanan, K. Dai, D.T. Haynie, Physica E 33 (2006) 92–98.
[82] H. Kudo, M. Fujihira, IEEE T. Nanotechnol. 5 (2006) 90–92.
[83] A.A. Zinchenko, K. Yoshikawa, D. Baigl, Adv. Mater. 17 (2005) 2820–2823.
[84] J.F. Liu, Y.L. Geng, E. Pound, A.T. Woolley, J.N. Harb, ACS Nano 5 (2011) 2240–2247.
[85] B. Uprety, J. Jensen, B.R. Aryal, R.C. Davis, A.T. Woolley, J.N. Harb, Langmuir 33 (2017) 10143–10152.
[86] S. Helmi, C. Ziegler, D.J. Kauert, R. Seidel, Nano Lett. 14 (2014) 6693–6698.
[87] W. Sun, E. Boulais, Y. Hakobyan, W.L. Wang, A. Guan, M. Bathe, et al., Science 346 (2014) 1258361, The experimental demonstration of casting metal nanoparticles with prescribed shapes within DNA nanostructures molds.
[88] K. Keren, R.S. Berman, E. Braun, Nano Lett. 4 (2004) 323–326.
[89] G.A. Burley, J. Gierlich, M.R. Mofid, H. Nir, S. Tal, Y. Eichen, et al., J. Am. Chem. Soc. 128 (2006) 1398–1399.
[90] M. Fischler, U. Simon, H. Nir, Y. Eichen, G.A. Burley, J. Gierlich, et al., Small 3 (2007) 1049–1055.
[91] C.T. Wirges, J. Timper, M. Fischler, A.S. Sologubenko, J. Mayer, U. Simon, et al., Angew. Chem. Int. Ed. 48 (2009) 219–223.
[92] S. Ganguly, S. Paul, O. Yehezkeli, J. Cha, M.H. Caruthers, Chem. Mater. 29 (2017) 2239–2245.
[93] K. Komizo, H. Ikedo, S. Sato, S. Takenaka, Bioconjugate Chem. 25 (2014) 1547–1555.
[94] Y. Weizmann, F. Patolsky, I. Popov, I. Willner, Nano Lett. 4 (2004) 787–792.
[95] B. Uprety, E.P. Gates, Y. Geng, A.T. Woolley, J.N. Harb, Langmuir 30 (2014) 1134–1141.
[96] S. Cui, Y. Liu, Z. Yang, X. Wei, Mater. Design 28 (2007) 722–725, The first experimental demonstration of electrochemical metallization on DNA.
[97] S. Jayaraman, W. Tang, R. Yongsunthon, J. Electrochem. Soc. 158 (2011) K123–K126.
[98] S.M. Watson, H.D. Mohamed, B.R. Horrocks, A. Houlton, Nanoscale 5 (2013) 5349–5359.
[99] A.O. Puchkova, P. Sokolov, Y.V. Petrov, N.A. Kasyanenko, J. Nanopart. Res. 13 (2011) 3633–3641.
[100] L. Berti, A. Alessandrini, P. Facci, J. Am. Chem. Soc. 127 (2005) 11216–11217, The first experimental demonstration of photochemical metallization on DNA.
[101] A.A. Zinchenko, N. Chen, S. Murata, Chem. Lett. 37 (2008) 1096–1097.
[102] M.M. Hossen, L. Bendickson, P.E. Palo, Z. Yao, M.N. Hamilton, A.C. Hillier, Nanotechnology 29 (2018) 355603.
[103] S.Y. Pu, A. Zinchenko, L.L. Qin, C.W. Ye, M. Xu, S. Murata, Mater. Lett. 130 (2014) 168–171.
[104] J. Samson, A. Varotto, P.C. Nahirney, A. Toschi, I. Piscopo, C.M. Drain, ACS Nano 3 (2009) 339–344.
[105] L. Yang, B. Sun, F. Meng, M. Zhang, X. Chen, M. Li, et al., Mater. Res. Bull. 44 (2009) 1270–1274.
[106] S. Kundu, H. Liang, Colloid. Surf. A 377 (2011) 87–96.
[107] A.H. Knoll, Rev. Mineral. Geochem. 54 (2003) 329–356.
[108] P.C.J. Donoghue, M.J. Benton, Trends Ecol. Evol. 22 (2007) 424–431.
[109] M. Numata, K. Sugiyasu, T. Hasegawa, S. Shinkai, Angew. Chem. Int. Ed. 116 (2004) 3341–3345.
[110] C.Y. Jin, H.B. Qiu, L. Han, M.H. Shu, S.A. Che, Chem. Commun. 23 (2009) 3407–3409.
[111] C.Y. Jin, L. Han, S.A. Che, Angew. Chem. Int. Ed. 48 (2009) 9268–9272.
[112] B. Liu, L. Han, S.A. Che, Angew. Chem. Int. Ed. 51 (2012) 923–927.
[113] X. Liu, F. Zhang, X. Jing, M. Pan, P. Liu, W. Li, et al., Nature 559 (2018) 593–598, The experimental demonstration of DNA origami silicification.
[114] L. Nguyen, M. Döblinger, T. Liedl, A.H. Jungemann, Angew. Chem. Int. Ed. (2019), http://dx.doi.org/10.1002/anie.201811323.
[115] S.L. Ginn, A.K. Amaya, I.E. Alexander, M. Edelstein, M.R. Abedi, J. Gene Med. 20 (2018), e3015.
[116] S. Surana, A.R. Shenoy, Y. Krishnan, Nat. Nanotechnol. 10 (2015) 741–747.
[117] Y.J. Chen, B. Groves, R.A. Muscat, G. Seelig, Nat. Nanotechnol. 10 (2015) 748–760.
[118] S. Katayose, K. Kataoka, Bioconjugate Chem. 8 (1997) 702–707.
[119] N.P. Agarwal, M. Matthies, F.N. Gur, K. Osada, T.L. Schmidt, Angew. Chem. Int. Ed. 56 (2017) 5460–5464.
[120] N. Ponnuswamy, M.M.C. Bastings, B. Nathwani, J.H. Ryu, L.Y.T. Chou, M. Vinther, et al., Nat. Commun. 8 (2017) 15654, The experimental demonstration of coating PEG on DNA origami to enhance the stability of origami.
[121] J.K. Kiviaho, V. Linko, A. Ora, T. Tiainen, E. Jarvihaavisto, J. Mikkila, et al., Nanoscale 8 (2016) 11674–11680.
[122] S.D. Perrault, W.M. Shih, ACS Nano 8 (2014) 5132–5140.
[123] S.P. Surwade, S. Zhao, H. Liu, J. Am. Chem. Soc. 133 (2011) 11868–11871.
[124] F. Zhou, B. Michael, S.P. Surwade, K.B. Ricardo, S. Zhao, H. Liu, Chem. Mater. 27 (2015) 1692–1698.
[125] C.T. Diagne, C. Brun, D. Gasparutto, X. Baillin, R. Tiron, ACS Nano 10 (2016) 6458–6463.
[126] S.H. Kang, W.S. Hwang, Z. Lin, S.H. Kwon, S.W. Hong, Nano Lett. 15 (2015) 7913–7920.
[127] F. Zhou, W. Sun, K.B. Ricardo, D. Wang, J. Shen, P. Yin, et al., ACS Nano 10 (2016) 3069–3077.
[128] Z. Jin, W. Sun, Y.G. Ke, C.J. Shih, G.L. Paulus, Q.H. Wang, et al., Nat. Commun. 4 (2013) 1663, The experimental demonstration of using metallized DNA nanostructures as plasma etching resist.
[129] B.X. Shen, V. Linko, K. Tapio, S. Pikker, T. Lemma, A. Gopinath, et al., Sci. Adv. 4 (2018), eaap8978.
[130] C. Lin, Y. Ke, Y. Liu, M. Mertig, J. Gu, H. Yan, Angew. Chem. Int. Ed. 46 (2007) 6089–6092.
[131] A.E. Gerdon, S.S. Oh, K. Hsieh, Y. Ke, H. Yan, H.T. Soh, Small 5 (2009) 1942–1946.
[132] A. Gopinath, E. Miyazono, A. Faraon, P.W. Rothemund, Nature 535 (2016) 401–405.
[133] R.J. Kershner, J.N. Cha, L.D. Bozano, C.T. Rettner, G.M. Wallraff, Nat. Nanotechnol. 4 (2009) 557–561.
[134] A. Kuzyk, B. Yurke, J.J. Toppari, V. Linko, P. Torma, Small 4 (2008) 447–450.
[135] B. Ding, H. Wu, W. Xu, Z. Zhao, Y. Liu, H. Yu, et al., Nano Lett. 10 (2010) 5065–5069.
[136] I. Gallego, B. Manning, J.D. Prades, M. Mir, J. Samitier, R. Eritja, Adv. Mater. 29 (2017), 1603233.
[137] A. Gopinath, P.W.K. Rothemund, ACS Nano 8 (2014) 12030–12040.
[138] A.J. Mastroianni, S.A. Claridge, A.P. Alivisatos, J. Am. Chem. Soc. 131 (2009) 8455–8459, The first experimental demonstration of creating chiral pyramids with AuNPs.
[139] W. Yan, L. Xu, C. Xu, W. Ma, H. Kuang, L. Wang, et al., J. Am. Chem. Soc. 134 (2012) 15114–15121.
[140] X.B. Shen, A.A. Garcia, Q. Liu, Q. Jiang, F.J.G. de A, N. Liu, et al., Nano Lett. 13 (2013) 2128–2133.
[141] G. Dai, X. Lu, Z. Chen, C. Meng, W. Ni, Q. Wang, ACS Appl. Mater. Interfaces 6 (2014) 5388–5392.
[142] M.Y.B. Zion, X.J. He, C.C. Maass, R.J. Sha, N.C. Seeman, P.M. Chaikin, Science 358 (2017) 633–636.
[143] X. Lan, Z. Chen, G. Dai, X. Lu, W. Ni, Q. Wang, J. Am. Chem. Soc. 135 (2013) 11441–11444, The first experimental demonstration of assembling 3D anisotropic AuNR dimers with DNA origami.
[144] X. Lan, X. Lu, C. Shen, Y. Ke, W. Ni, Q. Wang, J. Am. Chem. Soc. 137 (2015) 457–462.
[145] X. Shen, C. Song, J. Wang, D. Shi, Z. Wang, N. Liu, et al., J. Am. Chem. Soc. 134 (2012) 146–149.
[146] A. Kuzyk, R. Schreiber, Z. Fan, G. Pardatscher, E.M. Roller, A. Hogele, et al., Nature 483 (2012) 311–314, The experimental demonstration of assembling chiral plasmonic nanostructures on DNA helix.
[147] R. Schreiber, N. Luong, Z. Fan, A. Kuzyk, P.C. Nickels, T. Zhang, et al., Nat. Commun. 4 (2013) 2948.
[148] M.J. Urban, P.K. Dutta, P. Wang, X. Duan, X. Shen, B. Ding, et al., J. Am. Chem. Soc. 138 (2016) 5495–5498.
[149] Q. Jiang, Q. Liu, Y. Shi, Z.G. Wang, P. Zhan, J. Liu, et al., Nano Lett. 17 (2017) 7125–7130.
[150] A. Kuzyk, R. Schreiber, H. Zhang, A.O. Govorov, T. Liedl, N. Liu, Nat. Mater. 13 (2014) 862–866.
[151] C. Zhou, X. Duan, N. Liu, Nat. Commun. 6 (2015) 8102.
[152] S. Laing, L.E. Jamieson, K. Faulds, D. Graham, Nat. Rev. Chem. 1 (2017) 0060.
[153] E.C. Le Ru, P.G. Etchegoin, Single-molecule surface-enhanced Raman spectroscopy, in: M.A. Johnson, T.J. Martinez (Eds.), Annu. Rev. Phys. Chem, 2012, pp. 65–87.
[154] D.K. Lim, K.S. Jeon, J.H. Hwang, H. Kim, S. Kwon, Y.D. Suh, et al., Nat. Nanotechnol. 6 (2011) 452–460.
[155] D.K. Lim, K.S. Jeon, H.M. Kim, J.M. Nam, Y.D. Suh, Nat. Mater. 9 (2009) 60–67.
[156] J.W. Kang, P.T. So, R.R. Dasari, D.K. Lim, Nano Lett. 15 (2015) 1766–1772.
[157] M.P. Pais, A. Watson, S. Demers, T.H. LaBean, G. Finkelstein, Nano Lett. 14 (2014) 2099–2104, The first experimental demonstration of assembling AuNPs on DNA origami to enhance Raman signal.
[158] P. Kühler, E.M. Roller, R. Schreiber, T. Liedl, T. Lohmüller, J. Feldmann, Nano Lett. 14 (2014) 2914–2919.
[159] V.V. Thacker, L.O. Herrmann, D.O. Sigle, T. Zhang, T. Liedl, J.J. Baumberg, et al., Nat. Commun. 5 (2014) 3448.

[160] S. Simoncelli, E.M. Roller, P. Urban, R. Schreiber, A.J. Turberfield, T. Liedl, et al., ACS Nano 10 (2016) 9809–9815.
[161] S. Tanwar, K.K. Haldar, T. Sen, J. Am. Chem. Soc. 139 (2017) 17639–17648.
[162] P. Zhan, T. Wen, Z.G. Wang, Y. He, J. Shi, T. Wang, et al., Angew. Chem. Int. Ed. 57 (2018) 2846–2850.
[163] C.S. Yun, A. Javier, T. Jennings, M. Fisher, S. Hira, S. Peterson, et al., J. Am. Chem. Soc. 127 (2005) 3115–3119.
[164] G.P. Acuna, M. Bucher, I.H. Stein, C. Steinhauer, A. Kuzyk, P. Holzmeister, et al., ACS Nano 6 (2012) 3189–3195.
[165] J.V. Pellegrotti, G.P. Acuna, A. Puchkova, P. Holzmeister, A. Gietl, B. Lalkens, et al., Nano Lett. 14 (2014) 2831–2836.
[166] S.H. Ko, K. Du, J.A. Liddle, Angew. Chem. Int. Ed. 52 (2013) 1193–1197.
[167] P. Holzmeister, G.P. Acuna, D. Grohmann, P. Tinnefeld, Chem. Soc. Rev. 43 (2014) 1014–1028.
[168] A. Puchkova, C. Vietz, E. Pibiri, B. Wunsch, M.S. Paz, G.P. Acuna, et al., Nano Lett. 15 (2015) 8354–8359.
[169] I. Kaminska, J. Bohlen, S. Mackowski, P. Tinnefeld, G.P. Acuna, ACS Nano 12 (2018) 1650–1655.
[170] X.L. Zuo, C. Peng, Q. Huang, S.P. Song, L.H. Wang, D. Li, et al., Nano Res. 2 (2009) 617–623.
[171] O.I. Wilner, Y. Weizmann, R. Gill, O. Lioubashevski, R. Freeman, I. Willner, Nat. Nanotechnol. 4 (2009) 249–254.
[172] J. Fu, M. Liu, Y. Liu, N.W. Woodbury, H. Yan, J. Am. Chem. Soc. 134 (2012) 5516–5519.
[173] J.L. Fu, Y.R. Yang, A.J. Buck, M.H. Liu, Y. Liu, N.G. Walter, et al., Nat. Nanotechnol. 9 (2014) 531–536.
[174] Y. Fu, D. Zeng, J. Chao, Y. Jin, Z. Zhang, H. Liu, et al., J. Am. Chem. Soc. 135 (2013) 696–702.
[175] V. Linko, M. Eerikainen, M.A. Kostiainen, Chem. Commun. 51 (2015) 5351–5354.
[176] X. Huang, P.K. Jain, I.H. El-Sayed, M.A. El-Sayed, Lasers Med. Sci. 23 (2008) 217–228.
[177] W. Xu, J. Qian, G. Hou, Y. Wang, J. Wang, T. Sun, et al., Acta Biomater. 83 (2019) 400–413.
[178] Q. Guan, C. Wang, D. Wu, W. Wang, C. Zhang, J. Liu, et al., Nanotechnology 30 (2019).
[179] Q. Jiang, Y. Shi, Q. Zhang, N. Li, P. Zhan, L. Song, et al., Small 11 (2015) 5134–5141, The experimental demonstration of assembling DNA origami-AuNRs for photothermal therapy.
[180] Y. Du, Q. Jiang, N. Beziere, L. Song, Q. Zhang, D. Peng, et al., Adv. Mater. 28 (2016) 10000–10007.
[181] R. Crawford, C.M. Erben, J. Periz, L.M. Hall, T. Brown, A.J. Turberfield, et al., Angew. Chem. Int. Ed. 52 (2013) 2284–2288.
[182] X. Liu, Y. Xu, T. Yu, C. Clifford, Y. Liu, H. Yan, et al., Nano Lett. 12 (2012) 4254–4259.
[183] S.M. Douglas, I. Bachelet, G.M. Church, Science 335 (2012) 831–834.
[184] S. Li, Q. Jiang, S. Liu, Y. Zhang, Y. Tian, C. Song, et al., Nat. Biotechnol. 36 (2018) 258–264.
[185] Y. Tao, E. Ju, J. Ren, X. Qu, Chem. Commun. 49 (2013) 9791–9793.
[186] X. Michalet, F.F. Pinaud, L.A. Bentolila, J.M. Tsay, S. Doose, J.J. Li, et al., Science 307 (2005) 538–544.
[187] S. Wang, S. Deng, X. Cai, S. Hou, J. Li, Z. Gao, et al., Sci. China Chem. 59 (2016) 1519–1524.
[188] Z. Gao, S. Deng, J. Li, K. Wang, J. Li, L. Wang, et al., Sci. China Chem. 60 (2017) 1305–1309.
[189] G. Hong, J.T. Robinson, Y. Zhang, S. Diao, A.L. Antaris, Q. Wang, et al., Angew. Chem. Int. Ed. 51 (2012) 9818–9821.
[190] Y. He, Y.L. Zhong, Y.Y. Su, Y.M. Lu, Z.Y. Jiang, F. Peng, et al., Angew. Chem. Int. Ed. 50 (2011) 5695–5698.
[191] P. Wang, Y. Fan, L. Lu, L. Liu, L. Fan, M. Zhao, et al., Nat. Commun. 9 (2018) 2898.
[192] J. Zheng, R.M. Dickson, J. Am. Chem. Soc. 124 (2002) 13982–13983.
[193] J. Yu, S. Choi, R.M. Dickson, Angew. Chem. Int. Ed. 48 (2009) 318–320.
[194] Y. Wen, H. Pei, Y. Shen, J. Xi, M. Lin, N. Lu, et al., Sci. Rep. 2 (2012) 867.
[195] H.F. Sun, J. Chao, X.L. Zuo, S. Su, X.F. Liu, L. Yuwen, et al., RSC Adv. 4 (2014) 27625–27629.
[196] M.H. Lin, J.J. Wang, G.B. Zhou, J.B. Wang, N. Wu, J.X. Lu, et al., Angew. Chem. Int. Ed. 54 (2015) 2151–2155.
[197] Y. Su, T. Peng, F. Xing, D. Li, C. Fan, Acta Chim. Sinica 75 (2017) 1036–1046.
[198] D. Ye, X. Zuo, C. Fan, Prog. Chem. 29 (2017) 36–46.
[199] C.H. Fan, Y. Zhang, G.X. Li, J.Q. Zhu, D.X. Zhu, Electroanal. 12 (2000) 1156–1158.
[200] Z. Zhang, D.D. Zeng, H.W. Ma, G.Y. Feng, J. Hu, L. He, et al., Small 6 (2010) 1854–1858.
[201] D.W. Jacobsen, Clin. Chem. 44 (1998) 1833–1843.
[202] Y. Lin, Y. Tao, F. Pu, J. Ren, X. Qu, Adv. Funct. Mater. 21 (2011) 4565–4572.
[203] Z. Chen, L. Zhou, A. Zhao, Z. Zhang, Z. Wang, Y. Lin, et al., Biosens. Bioelectron. 58 (2014) 214–218.
[204] S. Hwang, E. Kim, J. Kwak, Anal. Chem. 77 (2005) 579–584.
[205] L. Wu, J. Wang, J. Ren, X. Qu, Adv. Funct. Mater. 24 (2014) 2727–2733.
[206] Q. Hu, W. Hu, J. Kong, X. Zhang, Biosens. Bioelectron. 63 (2015) 269–275.
[207] K. Keren, R.S. Berman, E. Buchstab, U. Sivan, E. Braun, Science 302 (2003) 1380–1382.
[208] G. Wang, A. Ishikawa, A. Eguchi, Y. Suzuki, S. Tanaka, Y. Matsuo, et al., ChemPlusChem 77 (2012) 592–597.
[209] A. Ongaro, F. Griffin, L. Nagle, D. Iacopino, R. Eritja, D. Fitzmaurice, Adv. Mater. 16 (2004) 1799–1803.
[210] S.G. Peera, A.K. Sahu, A. Arunchander, K. Nath, S.D. Bhat, J. Power Sources 297 (2015) 379–387.
[211] L.Y. Zhang, C.X. Guo, Z. Cui, J. Guo, Z. Dong, C.M. Li, Chem. Eur. J. 18 (2012) 15693–15698.
[212] D.J. Kim, M.A. Woo, Y.L. Jung, K.K. Bharathi, H.G. Park, D.K. Kim, et al., Nano Energy 8 (2014) 17–24.
[213] M.Z. Li, Y.X. Pan, X.Y. Guo, Y.H. Liang, Y.P. Wu, Y. Wen, et al., J. Mater. Chem. A 3 (2015) 10353–10359.
[214] K. Qu, L. Wu, J. Ren, X. Qu, ACS Appl. Mater. Interfaces 4 (2012) 5001–5009.
[215] J. Elbaz, P. Yin, C.A. Voigt, Nat. Commun. 7 (2016) 11179, The experimental demonstration of in vivo producing DNA tile structures.
[216] C. Kielar, Y. Xin, B. Shen, M.A. Kostiainen, G. Grundmeier, V. Linko, et al., Angew. Chem. Int. Ed. 57 (2018) 9470–9474.
[217] D.A. Giljohann, D.S. Seferos, P.C. Patel, J.E. Millstone, N.L.R. And, C.A. Mirkin, Nano Lett. 7 (2007) 3818–3821.
[218] Q. Jiang, C. Song, J. Nangreave, X. Liu, L. Lin, D. Qiu, et al., J. Am. Chem. Soc. 134 (2012) 13396–13403.

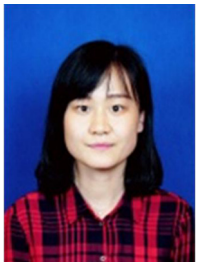

Yan Zhao obtained her B.S. degree from Shandong Normal University in 2012 and her Ph.D. degree from Shanghai Institute of Applied Physics, Chinese Academy of Sciences, in 2017. She is now a postdoctoral fellow. Her research interests are the functionalization and biological application of DNA nanostructures.

Xinpei Dai obtained her B.S. degree from Nanjing Tech University in 2017. She is now a postgraduate at Shanghai Institute of Applied Physics, Chinese Academy of Sciences. Her research interests include biomimetic mineralization and DNA nanotechnology.

Fei Wang obtained her B.S. from University of Science and Technology of China (USTC) in 2013. She obtained her Ph.D. from Shanghai Institute of Applied Physics, Chinese Academy of Sciences in 2018. During her PhD's studies, she went to UC Berkeley as a visiting scholar in 2017. Since 2018, she is in Prof. Chunhai Fan's group at Shanghai Jiao Tong University (SJTU) for postdoctoral research. Her research interests include DNA computing, CRISPR gene editing, super-resolution imaging and DNA nanotechnology.

Chunhai Fan obtained his B.S. and Ph.D. degree from Nanjing University in 1996 and 2000. After his postdoctoral research at the University of California, Santa Barbara, he joined the faculty at Shanghai Institute of Applied Physics, Chinese Academy of Sciences, in 2004. In 2018, he became a SJTU Chair Professor at Shanghai Jiao Tong University. His research interests include biosensors, biophotonics, DNA nanotechnology and DNA computation.

Xiaoguo Liu obtained his B.S. from Jilin University in 2008 and his Ph.D. from Shanghai Institute of Ceramics, Chinese Academy of Sciences, in 2013. From 2013–2018, he was a postdoctoral fellow and then an assistant professor at Shanghai Institute of Applied Physics. In 2018, he assumed a tenure track associate professor position at Shanghai Jiao Tong University. His research interests include inorganic biomaterials, biomimetic mineralization, DNA nanotechnology and synchrotron SAXS.